POLITECNICO DI TORINO

Department of Electronic and Telecommunications
Class LM-25 (DM270)

Master's Thesis in Mechatronic Engineering

Electromagnetic analysis and control of a six-phase low-voltage permanent-magnet synchronous motor for automotive powertrain

Tutors:
Prof. Andrea Tonoli
Prof. Renato Galluzzi
Eng. Raffaele Manca

Candidate:
Dario Puglisi

Academic Year 2023/2024

To Mery

Contents

Abstract

The adoption of low-voltage multiphase motors is a new trend in electric vehicles (EVs) for urban mobility and is an ideal choice for light electric vehicles designed for urban centres. At the design level, this emerging technology offer several advantages such as failsafe robustness, lower insulation costs and high compatibility with civil safety requirements and modularity. This thesis explores the design parameters and proposes an optimised control scheme for a dual three-phase electric motor with a hairpin construction powered by a 52V inverter. The motor is virtually modelled considering the influences of harmonics and losses by extrapolating the data calculated in Ansys Motor-CAD. The modelling of the control follows the Vector Space Decomposition (VSD) approach, the electrical quantities are represented in a vector space in 4 dimensions [d; q; z1; z2], paying attention to the optimisation of the torque required from the system efficiently by means of control techniques already known in literature for more classic three-phase motors. The proposed control guarantees the required torque tracking performance and can be implemented on a dual inverter system selected for the application, this structure lends itself to simulating case studies such as differences in battery voltages or faults of one of the two three-phase.

1. Introduction

This thesis project arises from the need to study a control for a multiphase PMSM electric motor to be implemented on an electric vehicle for urban mobility. The study and implementation of multi-phase electric motor is a new trend in recent years. The advantages of using this type of motor can be different. In this project, a 6-phase motor powered at low voltage will be considered, the automotive sector is interested in this technology as several advantages can be exploited to create new vehicle concepts for urban and sustainable mobility. A six-phase system offers significant advantages in terms of redundancy, allowing the motor to operate even in the presence of partial failures and thus improving vehicle resilience. Compared to high-voltage systems, a low-voltage motor has significant pros, including reduced electrical risks, lower insulation costs and greater compatibility with safety requirements for civil use. But a system defined in such a way introduces new issues that must be considered in the design of the motor control, such as increased mutual inductance influences that could compromise the correct conversion from current to torque or more in general efficiency. Different types of model and their relative control can be implemented, in this thesis the motor will be considered as a double three-phase model to simplify strategies and to be able to exploit the large literature already available for three-phase motors. In addition, the actual implementation of the motor involves the use of two inverters that manage each three-phase independently.

1.1. Vehicle concept project

Lately, research in the automotive world has been experimenting with new solutions for sustainable mobility, development of electric vehicles (BEVs) has supported the study of prototypes with new technologies to be deployed especially in urban centres. Supporting this background, this thesis works aims to study the motor and possible

control of a prototype electric vehicle, that is the result of a larger project that tends to bring together all new design technologies for the development of a car that is not currently on sale in the automotive market.

The main idea is to combine the safety and performance characteristics of M-class vehicles with the flexibility and cost-effectiveness of L-class vehicles. To achieve this, it is necessary to maintain a low weight and still be able to guarantee a good power density per weight. To meet these needs, the concept of an electric vehicle operating at low voltage (LVREV) is introduced, this idea also meets the principles of modularity, safety, accessibility and home integration. The vehicle features a 52 V architecture with two independent battery modules, connected to a six-phase electric motor via two inverters, which will be the subject of study in this thesis, as already mentioned. (1.1.)

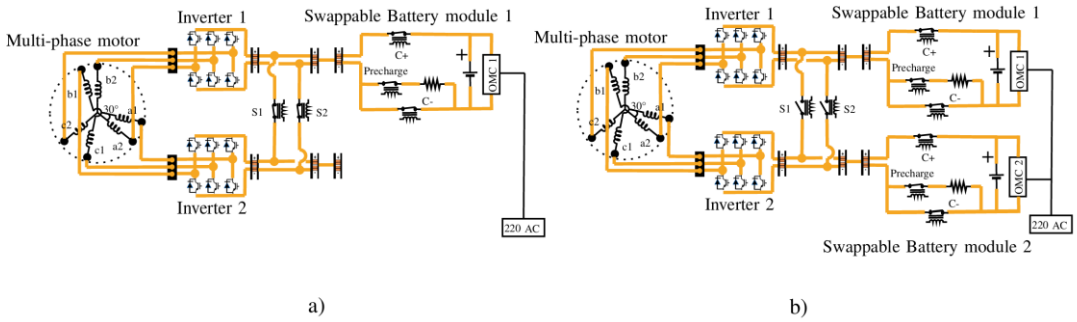

Figure 1 - Vehicle architecture a) Frugal configuration b) Dual configuration (1.1.)

The modularity principle is expressed in two modes of operation for vehicle system. In 'Frugal' mode, only one battery pack is used. In Dual mode, two battery packs are active for greater autonomy and performance. To make the two modes effective in both urban and non-urban usage scenarios, the design process uses simulations to optimise the efficiency of the electric drive module (EDM) and to determine the ideal battery pack size for the two vehicle configurations and the power required for the motor to achieve certain acceleration and torque performance.

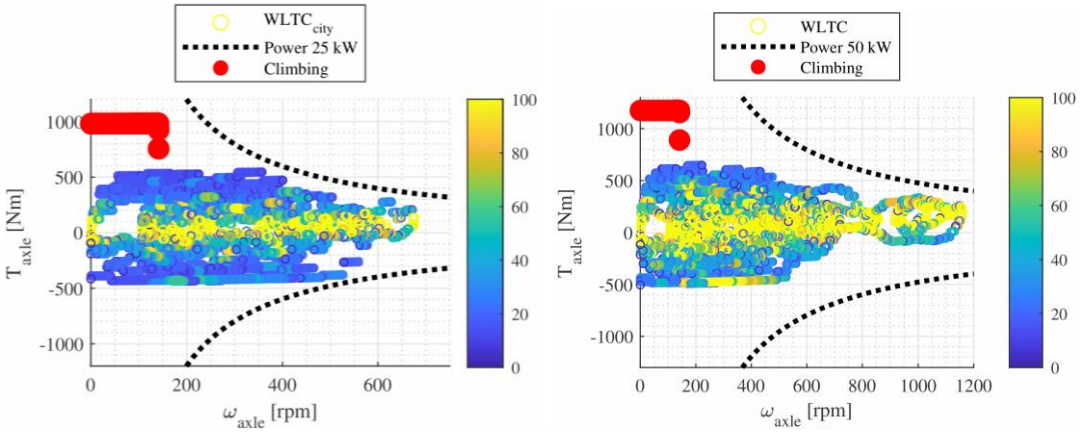

Figure 2 - Drive-cycles operational point in different scenario and configuration (1.1.)

	Frugal	Dual
Top speed	100 km/h	130 km/h
WLTC-City Range	192 km	-
Energy Cons. WLTC-City	8.2 kWh/100 km	-
WLTC Range	150 km	260 km
Energy Cons. WLTC	10.6 kWh/100 km	12.0 kWh/100 km
Voltage	52 V	52 V
Curb weight	870 kg	940 kg
GVW	1220 kg	1290 kg
Battery Size	15.8 kWh	31.6 kWh
Peak net power	30 kW	60 kW
Acc. time: $0-50$ km/h	5.3 s	5.3 s
Acc. time: $0-90$ km/h	14.5 s	10.9 s

Table 1 - Achieved result on drive-cycles simulation (1.1.)

Overall, the concept achieves the efficiency standards already present in vehicles for sale to the public but bridges the gap between L and M category vehicles, redefining a new model that is easily reconfigurable and scalable thanks to its flexibility.

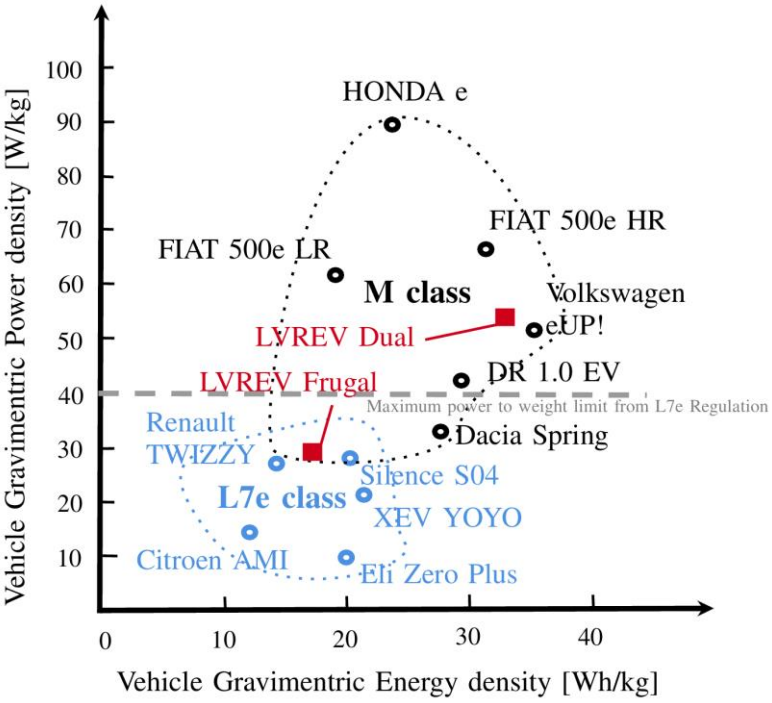

Figure 3 - BEVs comparison in terms of gravimetric energy and power density. (1.1.)

1.2. Magnetic Model

In PMSM the magnets produce a constant rotor flux, stator windings fed by current produce a rotating electromagnetic field, the interaction between the two electromagnetic field produces torque, according to:

$$T_{em} = \vec{B}_{stator} \times \vec{B}_{rotor}$$

In synchronous machines the rotating stator field must rotate at the same frequency as the permanent magnet field to obtain the maximum amount of torque stator and rotor magnetic field must be orthogonal. This condition must be considered in motor prototyping to reduce torque ripples and ensure a better dynamic response.

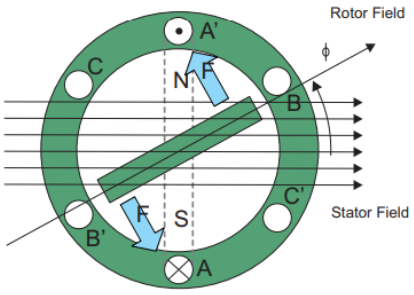

Figure 4 - Electromagnetic interaction between stator and rotor (1.2.)

The knowledge of the angle between stator and rotor θ is fundamental for a correct control of stator current to maintain the synchronous stator flux in quadrature with permanent flux.

1.2.1. ABC model

Considering a simple dual 3-phase machine, there will be the 6 magnetic axes, with double Y-connection and the 30° phase shift.

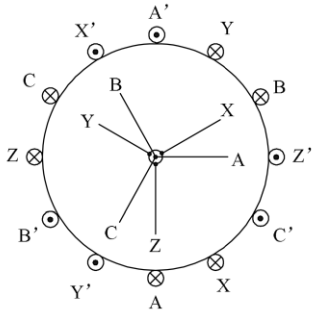

Figure 5 - Winding structure of six-phase double Y (3.1.)

The voltage equation in natural coordinates is:

$$\boldsymbol{u_s} = \boldsymbol{R_s i_s} + \frac{d\boldsymbol{\lambda_s}}{dt}$$

The flux equation is:

$$\boldsymbol{\lambda_s} = \boldsymbol{L_s i_s} + \gamma\lambda_{pm}$$

Where:

$$\boldsymbol{u_s} = [u_A\, u_B\, u_c\, u_X\, u_Y\, u_Z]^T\ ,\ \boldsymbol{i_s} = [i_A\, i_B\, i_C\, i_X\, i_Y\, i_Z]^T\ , \boldsymbol{\lambda_s} = [\lambda_A\, \lambda_B\, \lambda_C\, \lambda_X\, \lambda_Y\, \lambda_Z]^T,$$

$$\gamma = \left[cos\theta \quad \cos\left(\theta - \frac{2\pi}{3}\right) \quad \cos\left(\theta + \frac{2\pi}{3}\right) \quad \cos\left(\theta - \frac{\pi}{6}\right) \quad \cos\left(\theta - \frac{5\pi}{6}\right) \quad \cos\left(\theta + \frac{\pi}{2}\right)\right]^T$$

1.2.2. Transformation in dq axes

The static decoupling transformation matrix on vector space of the six-phase motor is:

$$T_{62s} = [\alpha, \beta, z1, z2, o1, o2]^T$$

This vector satisfies the following relationship

$$\begin{gathered} \alpha^T \cdot \beta = \ \alpha^T \cdot z1 = \ \alpha^T \cdot o1 = \ \alpha^T \cdot o2 = 0 \\ \beta^T \cdot z1 = \beta^T \cdot z2 = \ \beta^T \cdot o1 = \ \beta^T \cdot o2 = 0 \\ z1^T \cdot z2 = \ z1^T \cdot o1 = z1^T \cdot o2 = z2^T \cdot o1 = z2^T \cdot o2 = o1^T \cdot o2 = 0 \end{gathered}$$

Where α axis coincides with the A-phase winding axis, and β axis lags 90° compared with α-axis; α, β correspond to the sub-space associated with the electromechanical energy conversion; z1, z2 are the zero sequence and o1, o2 the homopolar terms. The four latter terms are not involved in the electromechanical energy conversion. Considering the transformation matrix which transforms the stationary α-β coordinate frame to the rotating d-q coordinate system, T can be determined by the multi-phase Clarke transformation. (3)

$$\boldsymbol{T}_{62r} = \begin{bmatrix} cos\vartheta & sin\theta & \mathbf{0} \\ -sin\theta & cos\theta & \mathbf{0} \\ \mathbf{0} & \mathbf{0} & \boldsymbol{I_4} \end{bmatrix}$$

The decoupled transformation matrix based on the vector space is:

$$\boldsymbol{T}_{62} = \begin{bmatrix} cos\theta & cos\left(\theta - \frac{2\pi}{3}\right) & cos\left(\theta + \frac{2\pi}{3}\right) & cos\cos\left(\theta - \frac{\pi}{6}\right) & cos\left(\theta - \frac{5\pi}{6}\right) & cos\left(\theta + \frac{\pi}{2}\right) \\ -sin\theta & -sin\left(\theta - \frac{2\pi}{3}\right) & -sin\left(\theta + \frac{2\pi}{3}\right) & -sin\cos\left(\theta - \frac{\pi}{6}\right) & -sin\left(\theta - \frac{5\pi}{6}\right) & -sin\left(\theta + \frac{\pi}{2}\right) \\ 1 & -\frac{1}{2} & -\frac{1}{2} & -\frac{\sqrt{3}}{2} & \frac{\sqrt{3}}{2} & 0 \\ 0 & -\frac{\sqrt{3}}{2} & \frac{\sqrt{3}}{2} & \frac{1}{2} & -\frac{1}{2} & -1 \\ 1 & 1 & 1 & 0 & 0 & 0 \\ 0 & 0 & 0 & 1 & 1 & 1 \end{bmatrix}$$

Taking the transformation matrix into the equation of the stationary coordinate system, considering that the isolation caused by the center line, o1-o2 subspace components are zero, the final voltage and flux equations can be written as:

$$\begin{bmatrix} u_d \\ u_q \\ u_{z1} \\ u_{z2} \end{bmatrix} = \begin{bmatrix} R_s & 0 & 0 & 0 \\ 0 & R_s & 0 & 0 \\ 0 & 0 & R_s & 0 \\ 0 & 0 & 0 & R_s \end{bmatrix} \begin{bmatrix} i_d \\ i_q \\ i_{z1} \\ i_{z2} \end{bmatrix} + \frac{d}{dt} \begin{bmatrix} \lambda_d \\ \lambda_q \\ \lambda_{z1} \\ \lambda_{z2} \end{bmatrix} + \omega \begin{bmatrix} -\lambda_q \\ \lambda_d \\ 0 \\ 0 \end{bmatrix}$$

$$\begin{bmatrix} \lambda_d \\ \lambda_q \\ \lambda_{z1} \\ \lambda_{z2} \end{bmatrix} = \begin{bmatrix} L_d & 0 & 0 & 0 \\ 0 & L_q & 0 & 0 \\ 0 & 0 & L_0 & 0 \\ 0 & 0 & 0 & L_0 \end{bmatrix} \begin{bmatrix} i_d \\ i_q \\ i_{z1} \\ i_{z2} \end{bmatrix} + \begin{bmatrix} 1 \\ 0 \\ 0 \\ 0 \end{bmatrix} \psi_{pm}$$

The electromagnetic torque of the six-phase in this model is:

$$T_e = 3p(i_q\lambda_d - i_d\lambda_q)$$

1.3. Modelling of multiphase drive, state of art

To implement a high-performance modulation and control strategy for multiphase drives (MPDs), an accurate model of a multiphase machine is essential. This section reviews various modeling approaches, with a particular focus on six-phase machines. Six-phase machines can have different winding configurations based on the spatial angle between two three-phase windings. Machines with a 60° angle are classified as symmetrical six-phase machines, while those with a 30° angle are referred to as asymmetrical six-phase machines. The asymmetrical six-phase machine, also known in the literature as a dual three-phase machine, offers advantages over its symmetrical counterpart, particularly in mitigating the fifth and seventh harmonics in the airgap flux. (1.3.)

1.3.1. Double DQ model

In the double-DQ model, the two three-phase windings of a six-phase machine are treated independently. Each set of phase variables undergoes a separate Clarke transformation. The α-axis of the stationary reference frame is aligned with phase-a1 of the stator winding. This process converts the six-phase variables into two sets of stationary reference frame components, labelled as $\alpha 1-\beta 1$ and $\alpha 2-\beta 2$, corresponding to the winding sets ABC1 and ABC2. (2.1.);(1.4.)

Considering for example the voltage, it will be mapped in this way:

$$[V_{\alpha j}\ V_{\beta j}]^{\,T} \;=\; [T_j] \cdot [V_{aj}\ V_{bj}\ V_{cj}]^T$$

The spatial 30° displacement between the two windings is accounted for in the decoupling transformation. For an asymmetrical six-phase machine, the power invariant transformation for winding sets ABC1 and ABC2, respectively, is given by:

$$T_1 = \sqrt{\frac{2}{3}}\begin{bmatrix} 1 & -\frac{1}{2} & -\frac{1}{2} \\ 0 & \frac{\sqrt{3}}{2} & -\frac{\sqrt{3}}{2} \end{bmatrix}$$

$$T_2 = \sqrt{\frac{2}{3}}\begin{bmatrix} \frac{\sqrt{3}}{2} & -\frac{\sqrt{3}}{2} & 0 \\ -1 & \frac{1}{2} & \frac{1}{2} \end{bmatrix}$$

1.3.2. Vector space decomposition model

The Vector Space Decomposition (VSD) method has recently become a popular approach for modelling multiphase AC machines (1.5.);(1.6.). Its primary goal is to transform the machine voltages and currents from their original six-dimensional space into new, independent subspaces. This transformation not only provides a unified

representation of machine dynamics but also facilitates the design of a more classical controller structure applicable in both healthy and faulty operating conditions.
According to decomposition theory, machine variables in the original six-dimensional space are projected into three mutually orthogonal subspaces: $\alpha\beta$, xy, and $0+0-$. The harmonics of the original vectors are grouped into these subspaces. The $\alpha\beta$ subspace captures the fundamental harmonic components and harmonics of order $\mathrm{k} = 12\mathrm{h} \pm 1$ with $(\mathrm{h} = 1,2,3,\dots)$. The $\alpha\beta$ current components are torque-producing, as they represent the fundamental harmonic. The xy subspace is associated with harmonics of order $\mathrm{k} = 6\mathrm{h} \pm 1$ with $(\mathrm{h} = 1,3,5,\dots)$, which spin in the same plane. These current components do not contribute to torque production and are considered as sources of additional losses under healthy conditions. However, in faulty conditions, they provide extra degrees of freedom for control purposes.
The $0+0-$ subspace corresponds to the triple harmonics, defined by $\mathrm{k} = 3\mathrm{h}$ with $(\mathrm{h} = 1,2,3,\dots)$. These current components only exist if a physical neutral path is available for the flow of neutral currents.
The transformation matrix used for this decomposition is:

$$T = \frac{1}{\sqrt{3}}\begin{bmatrix} 1 & -\frac{1}{2} & -\frac{1}{2} & \frac{\sqrt{3}}{2} & -\frac{\sqrt{3}}{2} & 0 \\ 0 & \frac{\sqrt{3}}{2} & \frac{\sqrt{3}}{2} & -\frac{1}{2} & \frac{1}{2} & -1 \\ 1 & -\frac{1}{2} & -\frac{1}{2} & -\frac{\sqrt{3}}{2} & \frac{\sqrt{3}}{2} & 0 \\ 0 & -\frac{\sqrt{3}}{2} & \frac{\sqrt{3}}{2} & \frac{1}{2} & \frac{1}{2} & -1 \\ 1 & 1 & 1 & 0 & 0 & 0 \\ 0 & 0 & 0 & 1 & 1 & 1 \end{bmatrix}$$

1.4. FOC Control Scheme

Considering a PMSM, the field orientated control (FOC) method represents an efficient way to drive a motor in a wide range of speeds. The main idea is to decouple the torque control and the magnetizing flux means a series of transformation. The DQ rotor current is injected as reference in control scheme, while the θ angle that represents the position of the rotor is used for the direct and inverse transformation in 3 - phases components. The correct measurement of θ is crucial for feedback control signal, a wrong estimation of that parameter could bring to drawbacks as alternating torque and consequently to an unwanted mechanical vibration of the rotor and more in general to low efficiency in the electromechanical conversion. (1.7.)

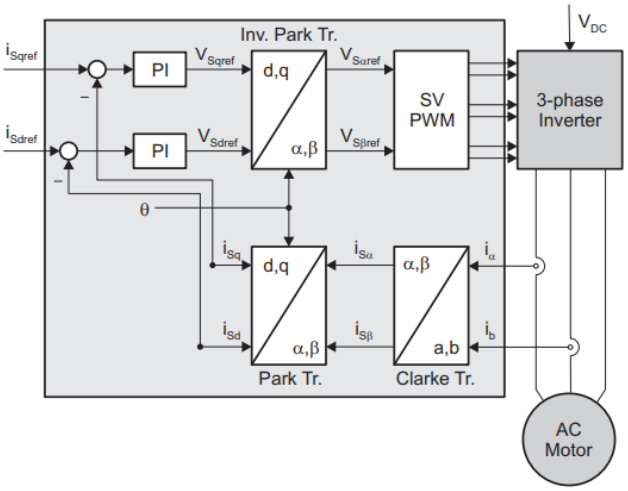

Figure 6 - Basic scheme FOC for AC machines (1.2.)

Furthermore, considering the DQ reference frame the torque expression become:

$$T \infty \lambda_R i_{sq}$$

This means it is possible to apply direct torque controlling the current in q axis, for this reason in a very naive control the current in d axis must be keep to zero because i_{sd} contributes only to generation of leakage flux.

1.4.1. Inverse transformation – open loop

The FOC structure scheme is a closed loop system, so the reference command current $(i_{sq}^{ref}; i_{sd}^{ref})$ are compared to feedback signals, then the error signals are regulated by means of two PI controllers.

Firstly, it is necessary to transform the regulated error $(V_{sq}^{ref}; V_{sd}^{ref})$ to a suitable quantity for the 3-phase inverter that will feed the AC motor.

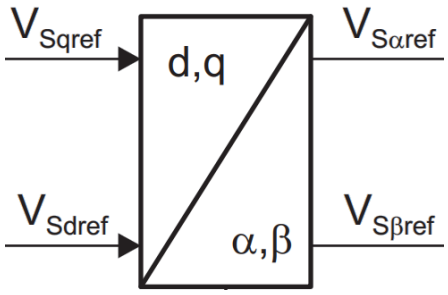

Figure 7 - Conversion block from dq to αβ (1.2.)

Inverse Park transformation is used to pass from dq to αβ reference frame.

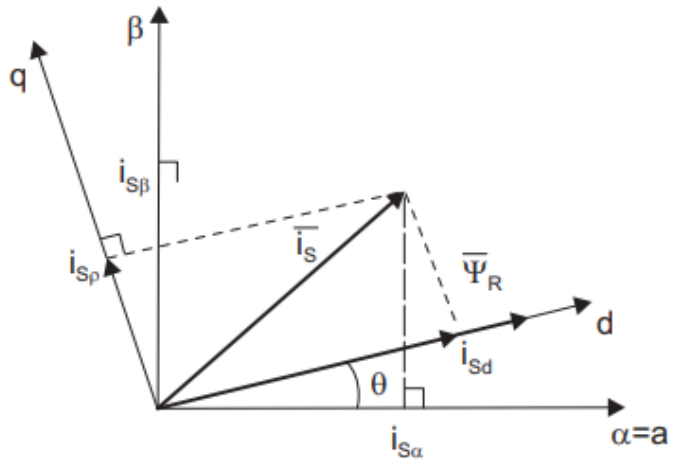

Figure 8 - Stator Current Space Vector and its component in αβ and in dq rotating frame (1.2.)

As said previously, for the transformation θ angle is fundamental and represent the relative position between the stationary and rotating reference frame.
The voltage $(V_{sq}^{ref}; V_{sd}^{ref})$ now it is used to generate the PWM command fot the inverter who drive the phases of the stator (in ABC reference frame)

1.4.2. Direct transformation – closed loop

From sensing between the inverter and the motor the current $(i_\alpha; i_\beta)$ is transformed in dq reference by a cascade of Clarke transformation and Park Transformation obtaining $(i_{sq}; i_{sd})$.

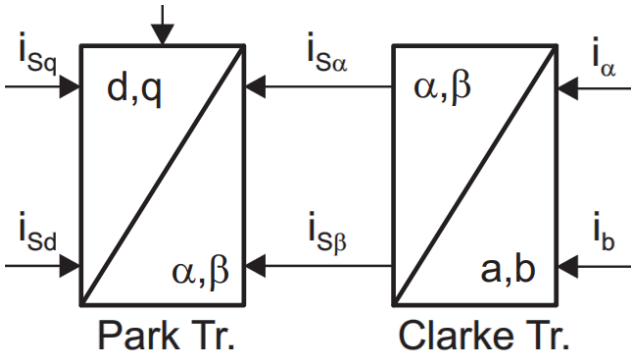

Figure 9 - Conversion blocks from αβ to dq (1.2.)

Now computed injected current in the stator is used as feedback in the FOC control scheme.

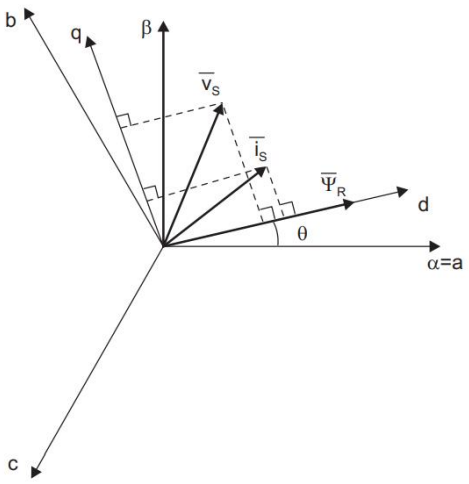

Figure 10 - Current, voltage and rotor flux space vectors in the dq rotating reference frame and their projection (1.2.)

The above Park transformation:

$$\begin{cases} i_{sd} = i_{s\alpha} \cdot cos\theta + i_{s\beta} \cdot sin\theta \\ i_{sq} = i_{s\alpha} \cdot sin\vartheta + i_{s\beta} \cdot cos\theta \end{cases}$$

recall again the importance of the correct estimation of θ angle for the sake of the whole control scheme. Rotor flux position is generally directly measured by a position sensor or by integration of rotor speed in synchronous machine.

1.5. Thesis Outline

In this first chapter, the context of the project requirement and the classical mathematical and control basics in the literature were introduced. In the following chapters, the same concepts will be applied and elaborated upon to analyse the models used to characterise the electrical motor and the Simscape structure for control. The fourth chapter will consider the numerical values obtained in the simulations. Finally, a final chapter will be used to express conclusions on the work carried out and possible improvements that can be implemented.

2. Motor Analysis

Electric motor drive units in commercial vehicles typically rely on parallel connections of modules to manage load current. However, this design leads to challenges such as imbalanced load sharing, timing differences during switching, and heat dissipation management. Multiphase drives distribute power across more phases, enabling each phase to operate independently with a single component, thereby reducing these issues. This approach simplifies thermal management and increases system efficiency, although it introduces added complexity due to the greater number of wires required.

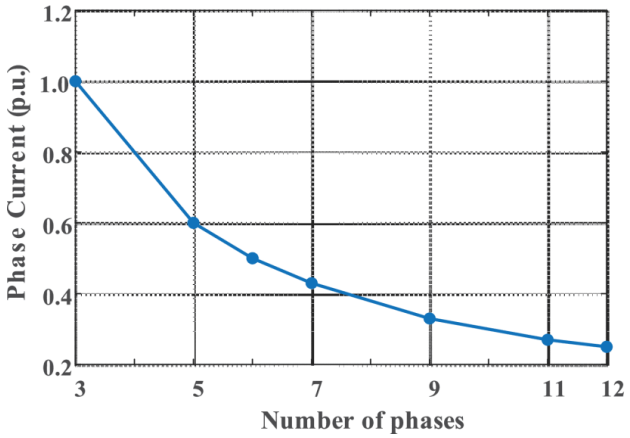

Figure 11 - Phase currents in p.u. for different MPDs (2.1.)

Multi-phase electric motor inherently provide better fault tolerance than traditional three-phase drives due to their higher phase count, which offers additional degrees of freedom during faults. This feature allows the system to maintain operation even with one or more faulty phases. Fault-tolerant designs optimize drive performance by focusing on criteria such as minimizing losses or maximizing torque under fault conditions. Advanced approaches also address the management of faults involving multiple phases, further enhancing system reliability. The histogram shown below shows the maximum torque values attainable in the event of a fault, for various differently configured MPDs.

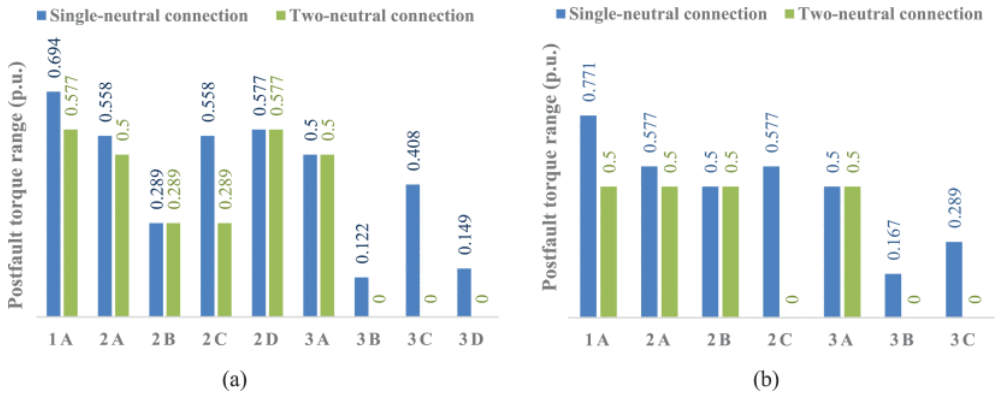

Figure 12 - Maximum postfault torque range in p.u. values under different faulty cases. (a) Asymmetrical and (b) symmetrical six-phase machines (2.2.)

MPDs can achieve higher torque density, making them ideal for applications requiring high-power-density motor drives, such as electric vehicles. Techniques like harmonic current injection improve torque production by utilizing subspaces in the machine's winding configurations. Challenges include managing the flow of harmonic currents and optimizing flux patterns in the machine's air gap. Solutions often involve advanced controllers to balance performance and minimize losses. Often, the dc-link capacitor bank is a critical component in electric vehicle powertrains, it account for a significant portion of converter size and cost. Increasing the number of phases in machine, reduces the required capacitance, so lowering the overall size and improving power density. For instance, a six-phase drive requires nearly half the capacitance of a comparable three-phase system, enhancing system compactness and efficiency. (2.1.)

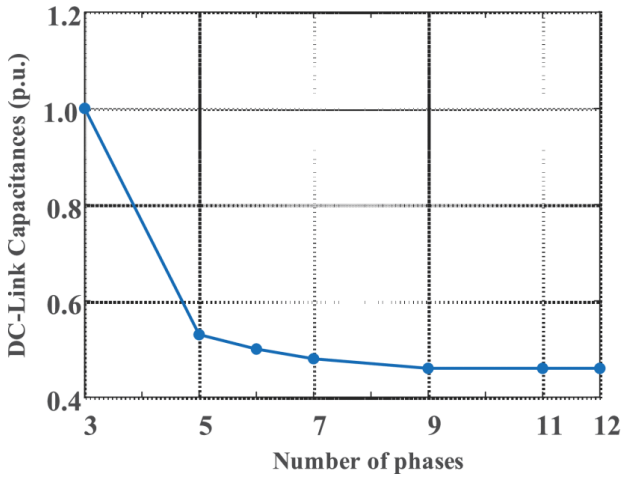

Figure 13 - Dc-Links capacitances in p.u. for different MPDs (2.3.)

2.1. Overview on multiphase motor model under test

The "Polito two spoke" is the electric motor on which this thesis project is based. This MPD is six-phase IPM with 52 V rated voltage. Has an asymmetrical displacement of winding, built with hairpin technology. Can be seen as a dual three-phase machine because each phase is shift by 30° with the phase of the other three-phase set.

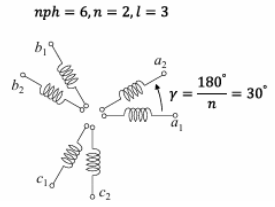

Figure 14 - Asymmetrical six-phase machine

The electric motor has two different neutral point, so we can supply the machine with one or multiple DC supply. Additionally, we can already take advantage of all the control methods used for 3-phase motors and related hardware, compared to multi-phase motors with independently connected phases or a single neutral point.

	Value
DC Supply Voltage	52 V
Maximum DC Vurrent	14 A/mm^2
Peak Output Power	60 kW
Peak Torque	93 Nm
Peak Speed	16000 rpm
Base Speed	5000 rpm
Slot Number	48
Pole Number	8
Stator Diameter	171 mm
Stator Length	100 mm
Avg. EM efficiency	92.5
Gear ratio	10.2

Table 2 - Electric drive module specification

2.1.1. VDS approch

The motor is analytically modelled according to the Vector Space Decomposition (VSD)

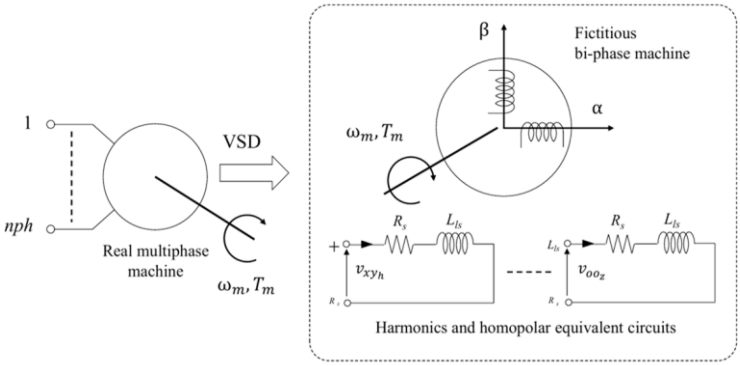

Figure 15 - VSD equivalent circuit (2.4.)

The choice of VSD approach decompose the machine with a reference transformation matrix in multiple orthogonal subspaces, makes possible the harmonic decoupling and considering homopolar components. The model in αβ reference system has the same equation of an equivalent 3-phase machine. This is the simplest approach that leverages harmonic subspaces to manage harmonics actively, minimizing losses and improving performance. In the following chapters, the mathematical transformations for the VSD modelling of the motoe will be analyzed in detail. (2.7.)

2.2. FEM parametrized machine models

One of the goals of the project is to create an almost equal model in MATLAB Simulink environment for reliable and consistent control, but at the same time easy to develop in order to test some possible scenarios in the application field.
The FEM analysis has been performed in Motor-cad software to trace with high fidelity the machine parameter of the machine. With E-magnetic computation it was possible calculate some parameters such as phase resistance, inductances and fluxes.

2.2.1. Efficiency map

Efficiency map is computed from Motor-cad simulation. From this data LUT for MTPA are extrapolated for successive motor control simulation.

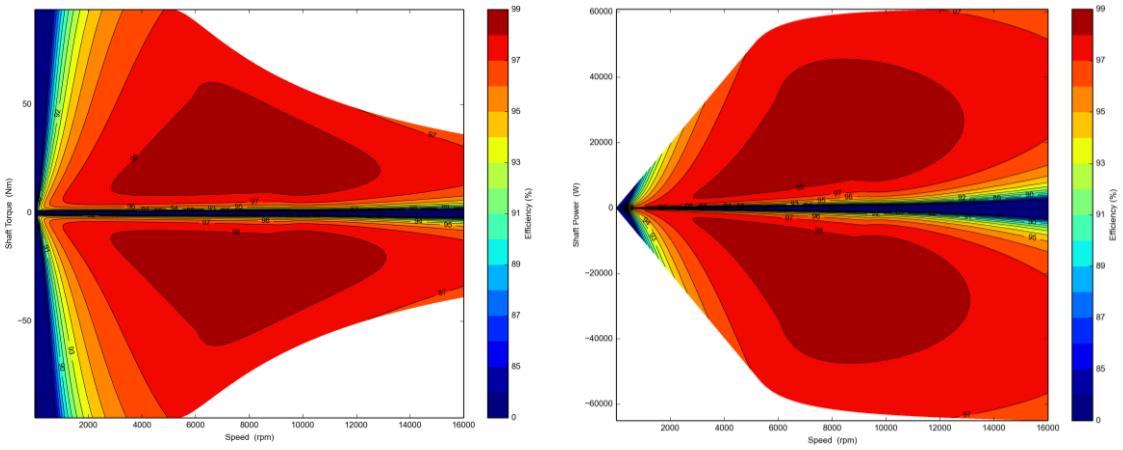

Figure 16 - Efficiency Map

2.2.2. Saturation and Loss map

Using the simulation tool in Ansys Motor-CAD, Saturation and Loss Map can be calculated. From the Saturation Map, the flux linkage for the D and Q axes and the electrical torque were obtained for each operating point of the electric motor, these values are useful for parameterising the motor in MATLAB. Loss Map were calculated to know the values such as Iron Losses, Eddy current coefficient for the stator and rotor, parametrized to vary peak current and rotor positions.

The simulation has been performed with these settings:

- Stator current peak from [0A 450A], with 50 A of step size
- Phase advance angle [-180° 180°], with 10° of step size
- Speed 1000 RPM

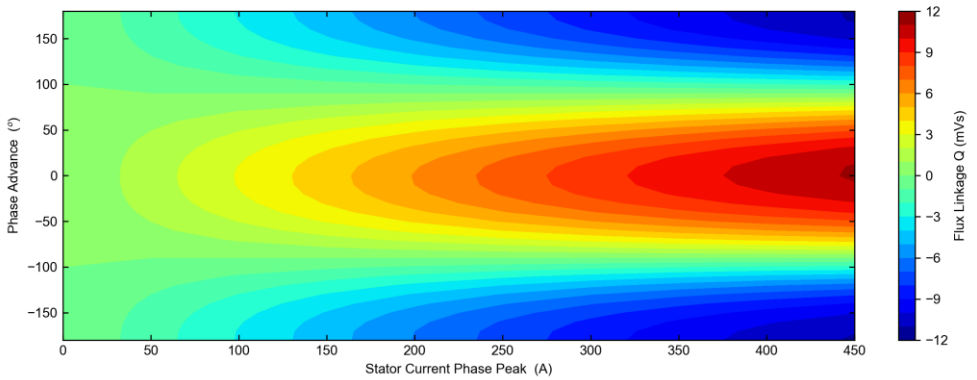

Figure 17 - Flux linkage Q axis

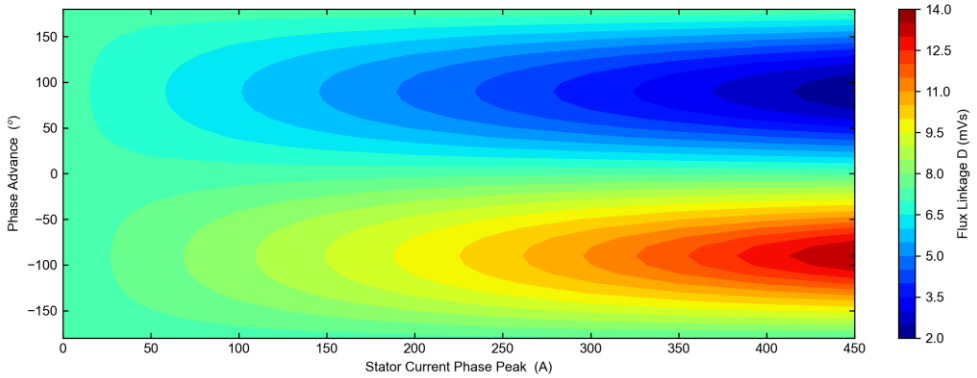

Figure 18 - Flux linkage D axis

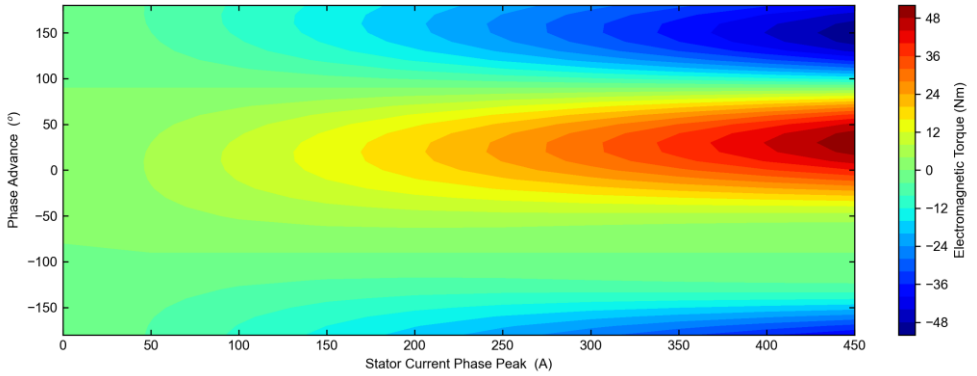

Figure 19 - Torque

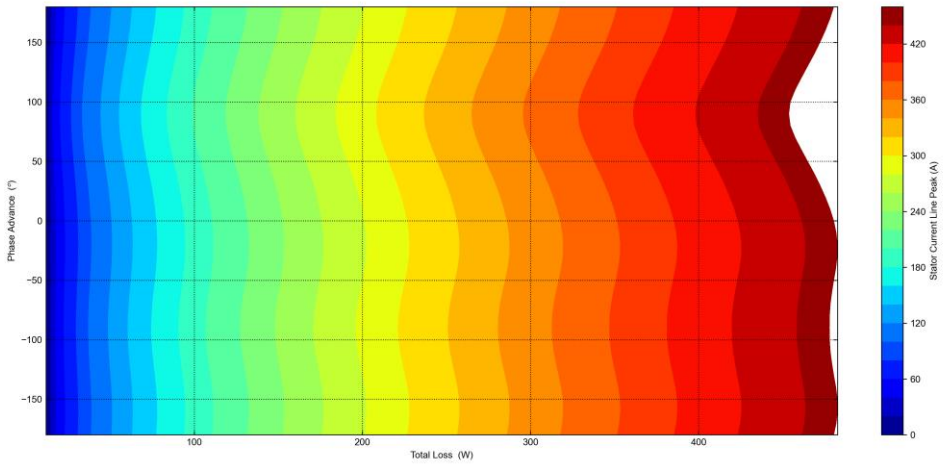

Figure 20 - Total Loss map

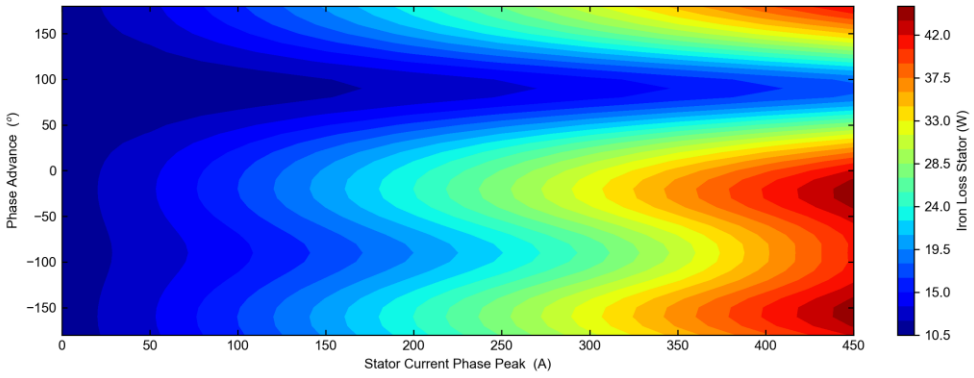

Figure 21 - Stator Iron Loss

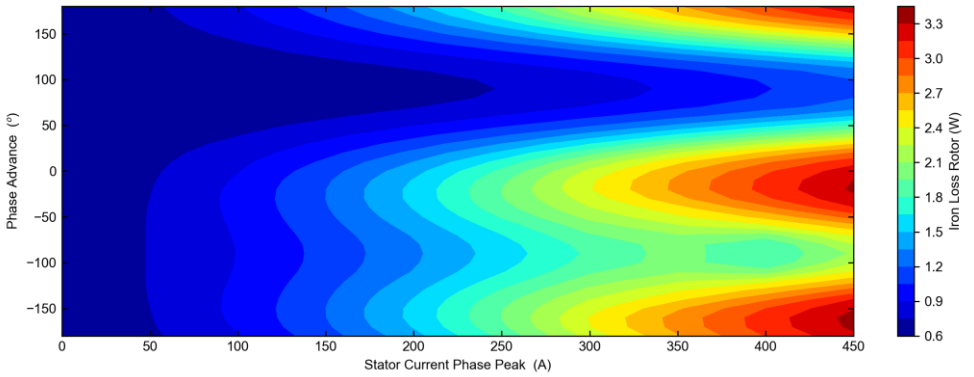

Figure 22 - Rotor Iron Loss

2.3.Customized Simulink motor block

By combining the data acquired from Motor-cad, it is possible to parameterise the Simscape "Dual three phase PMSM" block. This customizable Simscape component it is the result of a collaboration between Motor-cad and MATLAB for the prototyping in a Simulink environment of six-phase motors parameterised via FEM. In Simscape libraries it is already present a 'Six-phase PMSM' motor model, but it is modelled basically with static parameter there are characteristic of the motor as p, λ_m, L_d, L_q, L_0, R_s, J_r, this approach neglect the non idealities of the motor and propose a simplified linear version that is time-efficient in long simulations where the control has already been validated with a higher-precision model.

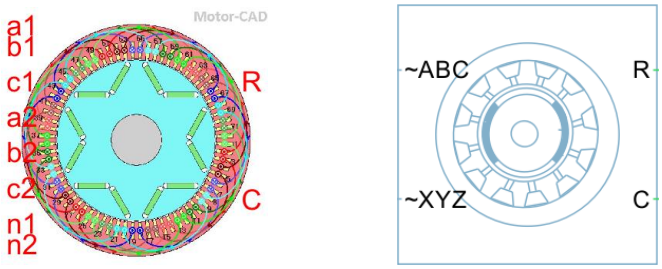

Figure 23 - Custom vs Standard Simscape block representation (2.5.)

The customized one is programmed via an ".ssc" script that contains all the power port indications and equations governing the block. The script has a graphic equivalent window that shows which variables are used in the parameterisation. Below you can see the MATLAB variables that parameterise the model. The matrices have been directly exported from Ansys Motor-CAD and are loaded into the MATLAB workspace via an additional script that appropriately formats the dimensions as required by the block.

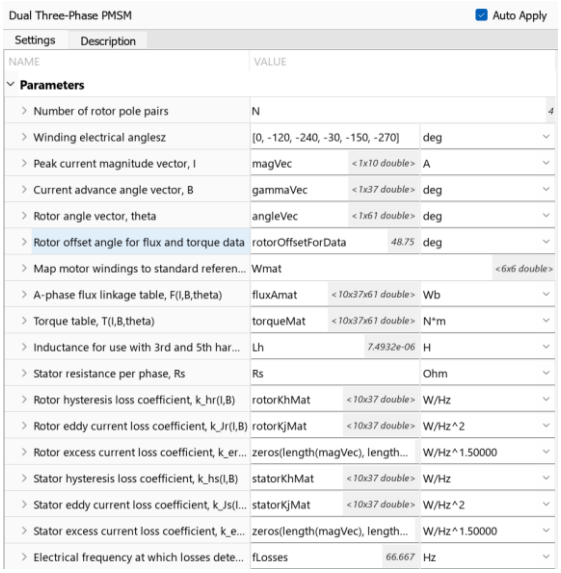

Figure 24 - Dual Three-phase PMSM parametrization

The approach used for mathematical modelling in the block is Vector Space Decomposition (VDS). The data of a single phase are arranged via the W matrix to comply the conventional winding configuration.

$$\begin{bmatrix} i_1 \\ i_2 \\ i_3 \\ i_4 \\ i_5 \\ i_6 \end{bmatrix} = W \begin{bmatrix} i_{A1} \\ i_{B1} \\ i_{C1} \\ i_{A2} \\ i_{B2} \\ i_{C2} \end{bmatrix} = \begin{bmatrix} 1 & 0 & 0 & 0 & 0 & 0 \\ 0 & 0 & 0 & 1 & 0 & 0 \\ 0 & 0 & -1 & 0 & 0 & 0 \\ 0 & 0 & 0 & 0 & 0 & -1 \\ 0 & 1 & 0 & 0 & 0 & 0 \\ 0 & 0 & 0 & 0 & 1 & 0 \end{bmatrix} \begin{bmatrix} i_{A1} \\ i_{B1} \\ i_{C1} \\ i_{A2} \\ i_{B2} \\ i_{C2} \end{bmatrix}$$

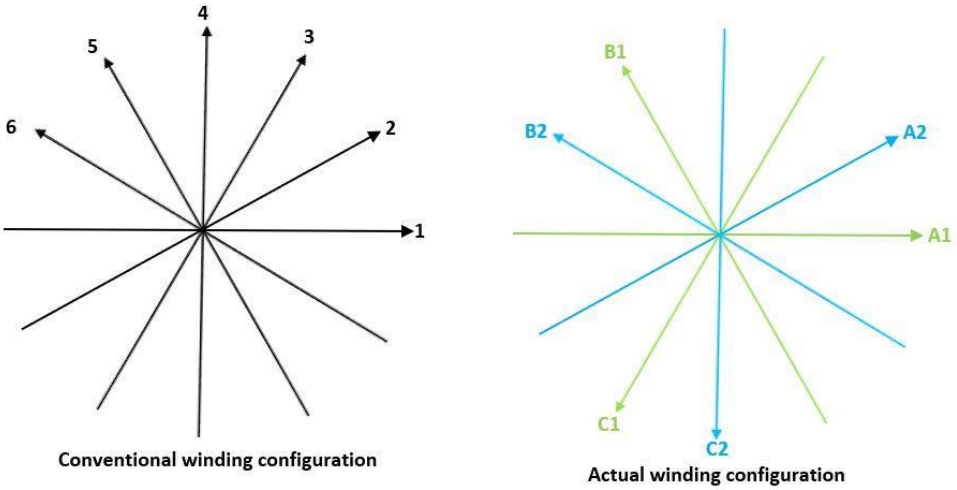

Figure 25 - Winding configuration (2.5.)

Once in the conventional winding configuration, the Clarke transform maps magnetic field contributions from windings 1 to 6 to a net total resolved into the axis of first winding, and an axis perpendicular to it. Denoting the angle between phases as $\alpha = \frac{\pi}{6}$ and by considering the geometry of the conventional winding configuration, the Clarke transform can be written out as:

$$C = \frac{2}{6}\begin{bmatrix} 1 & \cos\alpha & \cos 2\alpha & \cos 3\alpha & \cos 4\alpha & \cos 5\alpha \\ 0 & \sin\alpha & \sin 2\alpha & \sin 3\alpha & \sin 4\alpha & \sin 5\alpha \end{bmatrix}$$

This definition of Clarke's transform will only take account of currents at the fundamental frequency. As there are six windings, there are six dynamic states associated with stator inductances. This means that we need to include the 3rd and the 5th harmonics if mapping the stator dynamics to rotor axes, this giving a total of six dynamics states in rotor axes. To do this, the Clarke transform is appended with four more rows that take account of the additional harmonics:

$$C_{135} = \frac{2}{6}\begin{bmatrix} 1 & \cos\alpha & \cos 2\alpha & \cos 3\alpha & \cos 4\alpha & \cos 5\alpha \\ 0 & \sin\alpha & \sin 2\alpha & \sin 3\alpha & \sin 4\alpha & \sin 5\alpha \\ 1 & \cos 3\alpha & \cos 6\alpha & \cos 9\alpha & \cos 12\alpha & \cos 15\alpha \\ 0 & \sin 3\alpha & \sin 6\alpha & \sin 9\alpha & \sin 12\alpha & \sin 15\alpha \\ 1 & \cos 5\alpha & \cos 10\alpha & \cos 15\alpha & \cos 20\alpha & \cos 25\alpha \\ 0 & \sin 5\alpha & \sin 10\alpha & \sin 15\alpha & \sin 20\alpha & \sin 25\alpha \end{bmatrix}$$

The total fluxes resolved into a stationary reference frame, that consists of the orthogonal axis set referred to the A1-phase winding axis. The stationary reference frame can now transform into a rotational reference frame fixed to the rotor and with two orthogonal rotor axes using Park's transform.
The imported flux linkage has been generated using the original Park's transform for which the q-axis leads the d-axis, rotor angle is measured from the A1-phase to the q-axis, and amplitude-invariant normalization is applied. This convention is shown in the figure below. (2.5.)

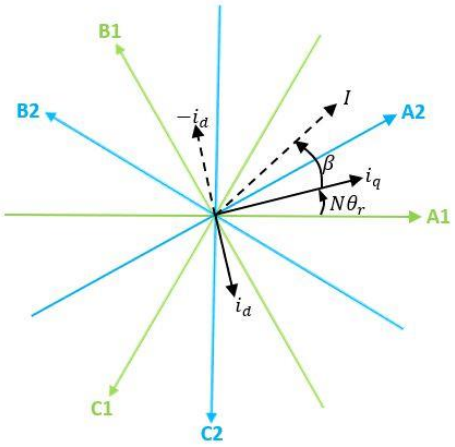

Figure 26 - Definition of rotor quantities relative to stator (2.5.)

The current phase advance angle is defined using q-axis as reference with the relation:

$$B = \tan^{-1}\frac{i_d}{i_q}$$

and current magnitude is defined as:

$$I = \sqrt{i_d^2 + i_q^2}$$

Fluxes and torque are tabulated in terms of current phase advance angle, current magnitude, and rotor electrical angle. Rotor electrical angle is rotor angle θ_r multiplied by the number of rotor pole pairs N.
Park's transform rotating from reference frame to rotor axes is:

$$P = \begin{bmatrix} \sin N\theta_r & -\cos N\theta_r \\ \cos N\theta_r & \sin N\theta_r \end{bmatrix}$$

Extending this definition to include the 3rd and 5th harmonics gives:

$$P_{135} = \begin{bmatrix} \sin N\theta_r & -\cos N\theta_r & 0 & 0 & 0 & 0 \\ \cos N\theta_r & \sin N\theta_r & 0 & 0 & 0 & 0 \\ 0 & 0 & \sin 3N\theta_r & -\cos 3N\theta_r & 0 & 0 \\ 0 & 0 & \cos 3N\theta_r & \sin 3N\theta_r & 0 & 0 \\ 0 & 0 & 0 & 0 & \sin 5N\theta_r & -\cos 5N\theta_r \\ 0 & 0 & 0 & 0 & \cos 5N\theta_r & \sin 5N\theta_r \end{bmatrix}$$

The total transformation from stator to rotor quantities is then given by:

$$T_{135} = P_{135} C_{135} W$$

Hence:

$$\begin{bmatrix} \psi_d \\ \psi_q \\ \psi_{\mathrm{d3}} \\ \psi_{\mathrm{q3}} \\ \psi_{\mathrm{d5}} \\ \psi_{\mathrm{q5}} \end{bmatrix} = T_{135} \begin{bmatrix} \psi_{\mathrm{A1}} \\ \psi_{\mathrm{B1}} \\ \psi_{\mathrm{C1}} \\ \psi_{\mathrm{A2}} \\ \psi_{\mathrm{B2}} \\ \psi_{\mathrm{C2}} \end{bmatrix}$$

The motor fluxes depend on six currents plus rotor angle. To tabulate fluxes in seven dimensions is computationally impractical. Hence, to reduce this complexity, fluxes are tabulated as a function only of fundamental frequency currents i_q and i_d plus rotor angle. This is then augmented by the 3rd and 5th harmonic inductances to model behavior when the system state is perturbed away from perfectly balanced stator currents.(2.6.) The required equation is as follows:

$$\begin{bmatrix} e_{\mathrm{A1}} \\ e_{\mathrm{B1}} \\ e_{\mathrm{C1}} \\ e_{\mathrm{A2}} \\ e_{\mathrm{B2}} \\ e_{\mathrm{C2}} \end{bmatrix} = \frac{d}{\mathrm{dt}} \left(\begin{bmatrix} \psi_{\mathrm{A1}}(I, B, \theta) \\ \psi_{\mathrm{B1}}(I, B, \theta) \\ \psi_{\mathrm{C1}}(I, B, \theta) \\ \psi_{\mathrm{A2}}(I, B, \theta) \\ \psi_{\mathrm{B2}}(I, B, \theta) \\ \psi_{\mathrm{C2}}(I, B, \theta) \end{bmatrix} + T_{135}{}^{-1} \begin{bmatrix} 0 \\ 0 \\ L_3\, i_{\mathrm{d3}} \\ L_3\, i_{\mathrm{q3}} \\ L_5\, i_{\mathrm{d5}} \\ L_5\, i_{\mathrm{q5}} \end{bmatrix} \right)$$

2.4. Equivalence with Motor-cad model E-magnetic simulation

Before implementing the block in a control scheme, a model validation was performed to check whether all entered parameters led to a 1:1 correspondence of the model with Ansys Motor-CAD values.

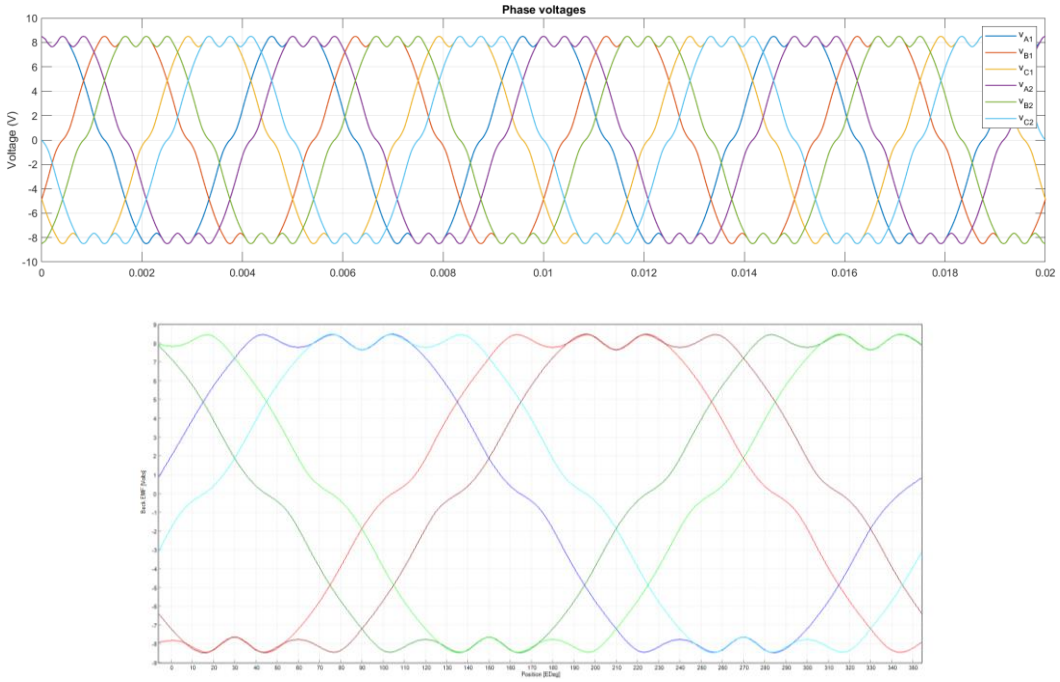

Figure 27 - Back EMF comparison between Motor-CAD and Simulink

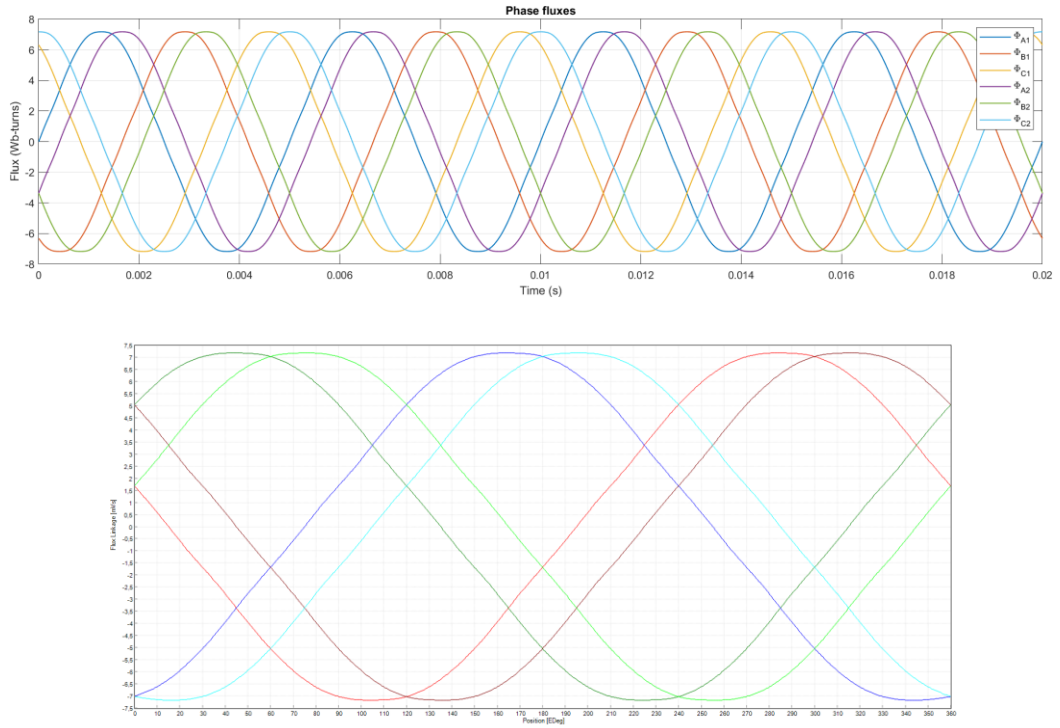

Figure 28 - Flux linkage comparison between Motor-CAD and Simulink

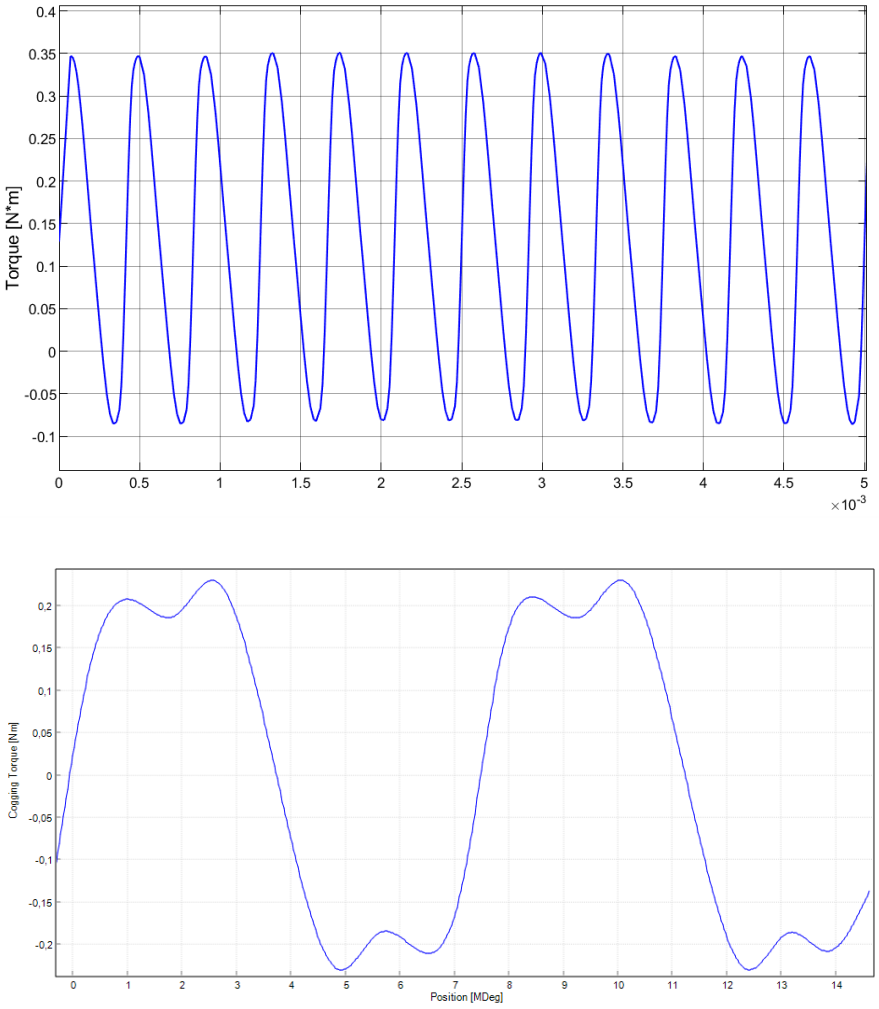

Figure 29 - Cogging torque comparison between Motor-CAD and Simulink

The results show an excellent match in waveforms and amplitudes for back EMF and flux linkages. These results are possible due to the addition to the model of current influences in 3rd and 5th harmonics and loss parameters that are neglected in standard models. Only the cogging torque presents a variation in the waveform and an offset from the values found in Motor-CAD, this result is to be considered as a non-ideality not handled by the block. (2.8.)

3. Control

Motor control represent the main part of the project. There are various structures and ways in which the control can be carried out, each of which tends to favour or limit the response to signals imposed as references in different ways.

Two approaches were used as control schemes in the project:

- Current control in the q-axis
- MTPA based control

The first approach is the simplest, but effective. It imposes all the current in the Q-axis and thus succeeds in providing great dynamics to the system even if not in an optimised manner. The second approach imposes currents via the LUTs exported by Motor-CAD, so better current management is expected for electric torque generation. In both cases, the currents in Z1 and Z2 are imposed at zero to try to control current imbalances due to inequalities in the motor geometries that result in parasitic electromagnetic effects.

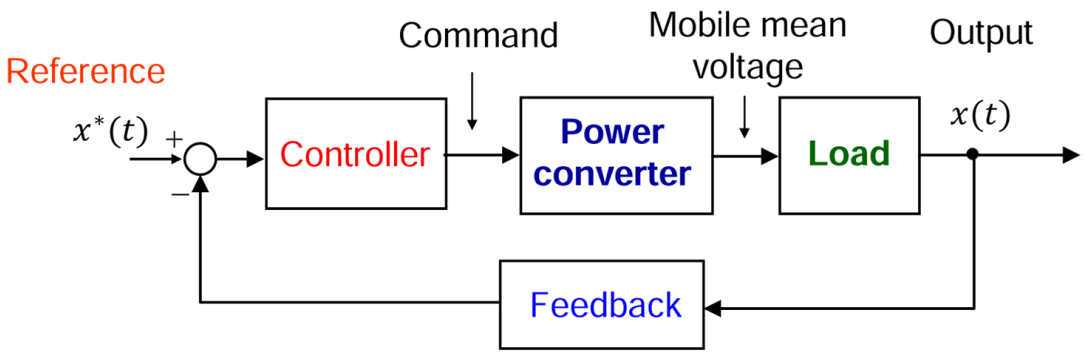

Figure 30 - System block scheme

The reference control scheme is the same showed in figure 6 in the first chapter.

Analysing the open chain, there are the three basic components for drawing control. The load represents the motor in the screen, the power converter represents the single three-phase inverter, and the control is basically the PI regulator and saturations. All these components must be modelled correctly considering characteristic values such as the sampling time of the system and the switching frequency of the inverter. PI tuning is a crucial step for correct torque tracking.

The command value is basically the six step vector to pilot the power converter, to reach the output request of voltage. There are total of 64 space vectors in the six-phase inverter, graphically showed above:

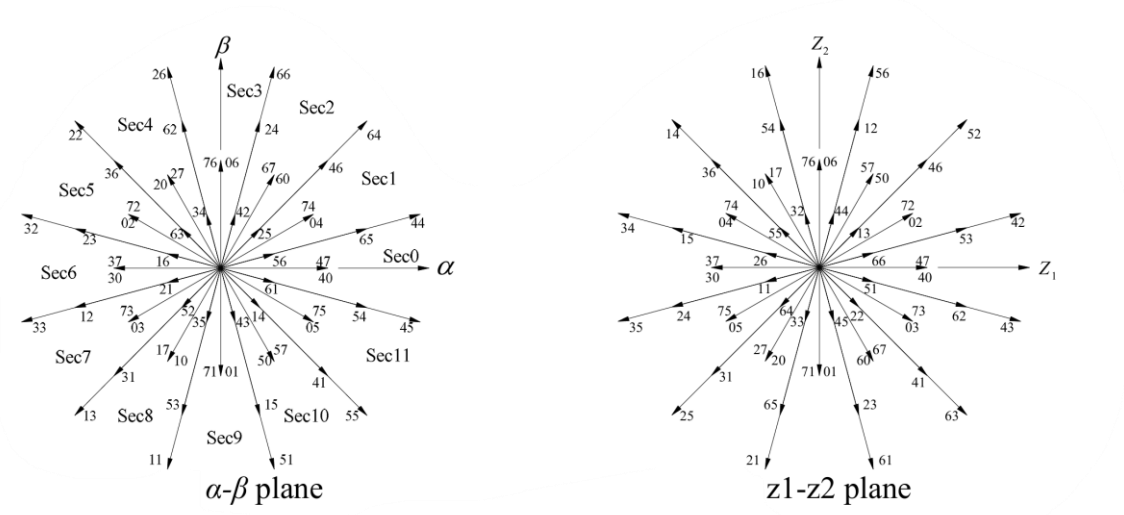

Figure 31 - Diagram of six phase inverter voltage vectors (3.1)

We recall also the voltage equation in DQ axis that represents the reference voltage value derived from current request:

$$v_d = R_s i_d + L_d \frac{di_d}{dt} - \omega L_q i_q$$

$$v_q = R_s i_q + L_d \frac{di_q}{dt} - \omega (L_d i_d + \lambda_{pm})$$

In all the strategies adopted, the voltage reference in Z1 and Z2 is set to zero for simplicity, so the task of the PI controllers is to keep the current vector in these two axes as small as possible. Recall that zero injection operations serve to reduce the unbalances experienced by three-phase drives and do not contribute to electromechanical conversion, so a more evolved control could implement synchronous PIs, capable of providing better performance. An important consideration is that the flux of the permanent magnets cannot be measured directly, so a flux weaking will be introduced into the control to incorporate this dynamic contribution.

3.1. Simulink control scheme analysis

The schematic consisting of three fundamental elements:

- The electrical and mechanical
- The control
- Input signals and scopes for visualisation

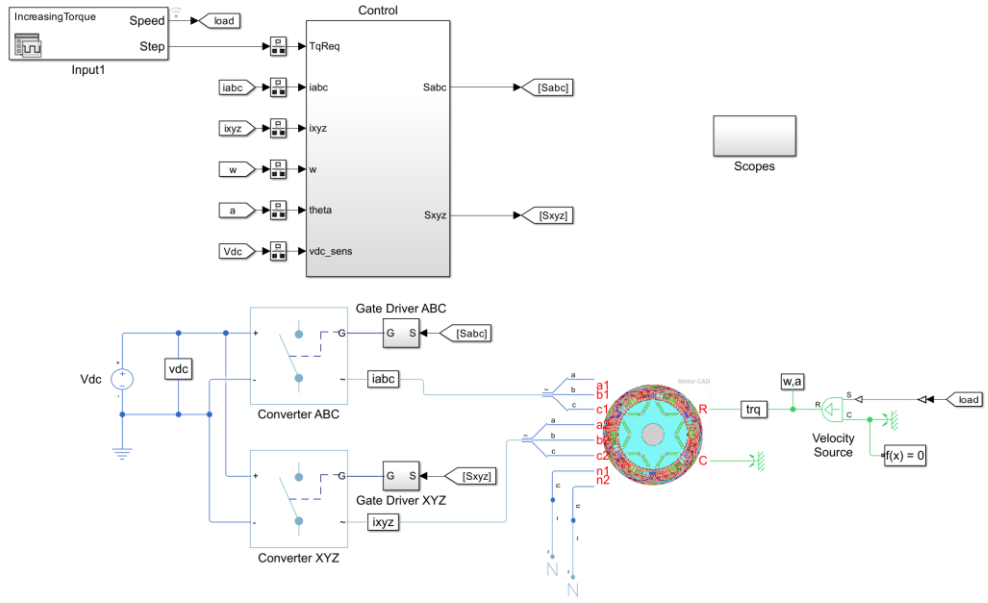

Figure 32 - Main Simulink Interface

The schematic follows the basic structure of the FOC, transforming the demand for torque and speed (rpm) into appropriately controlled signals to drive the inverters that will power the motor phases. There is no control loop for velocity, which is always generated by the velocity source. This choice allows control to be focused and optimized on torque as the only variable.

The two three-phase converters on ABC and XYZ are modelled as three-phase inverters based on MOSFET devices, driven by PWM signals (SVM) generated in the control block. The 'Control' block consists of two basic subsystems:

- Outer Loop Control
- Current Control

In the first subsystem, the torque reference is transformed into desiring currents in the Q, D, Z1, Z2 axes. This block differs in the two control strategies tested.
In the second subsystem the computed reference currents are compared with feedback measure:

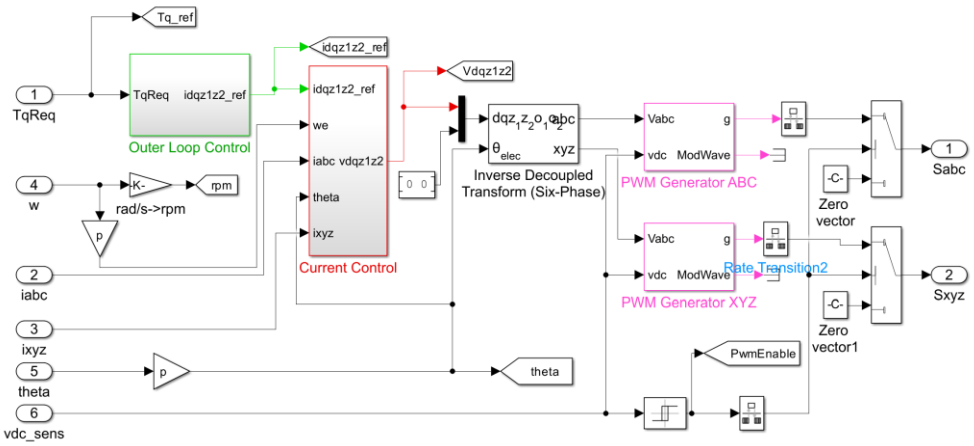

Figure 33 - Control block

In the 'current regulator block', as can be seen below, PI regulators are implemented and a 'DQ limiter' is cascaded for the Q and D branches. The action of the DQ limiter is very important because it imposes dynamic damping to attenuate very abrupt changes in torque demand. In addition, it is possible to prioritize the current in one of the two axes or maintain a balance, the possibility of choice is reflected in a more refined tuning of the control. The choice of the best setting for the DQ limiter varies depending on the operations to be performed by the motor.
Another crucial function for this subsystem is the feedforward action applied to D and Q to introduce the dynamical influences in voltage equation of the motor. Z1 and Z2 current are regulated by simply PI regulator.

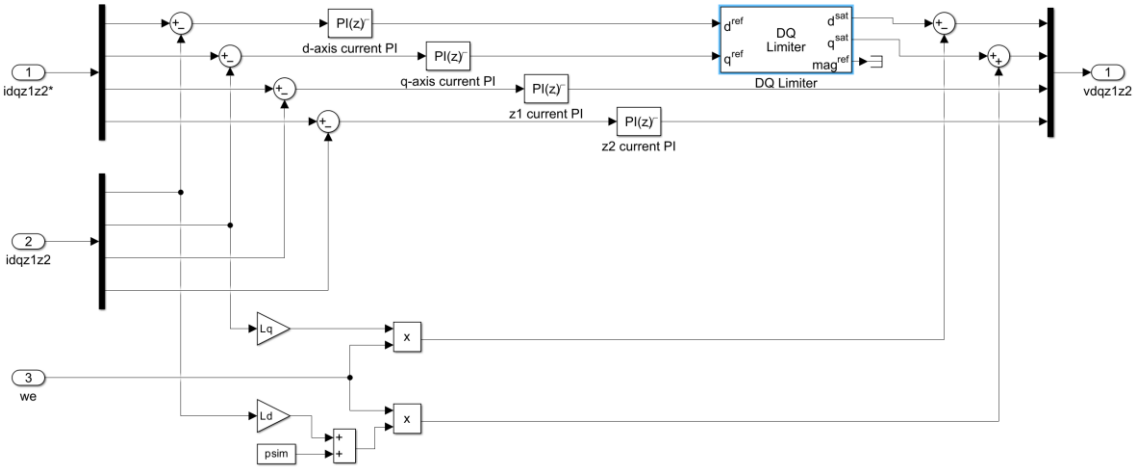

Figure 34 - PI control subsystem (Current control)

3.1.1. Control only in Q-axis

$$T_e = 3 \cdot p \cdot i_q \cdot \lambda_d$$

Then, imposing zero current in d axis, the flux on d depends only on permanent magnets, so the equation become:

$$T_e = 3 \cdot p \cdot i_q \cdot \lambda_m$$

rewriting the equation for the current in q, we obtain:

$$i_q = \frac{T_e}{3 \cdot p \cdot \lambda_m}$$

In this control method the only control variable is the q current, the others current branches are set to zero. Below there is the modified FOC schematic in case of only q-axis current control.

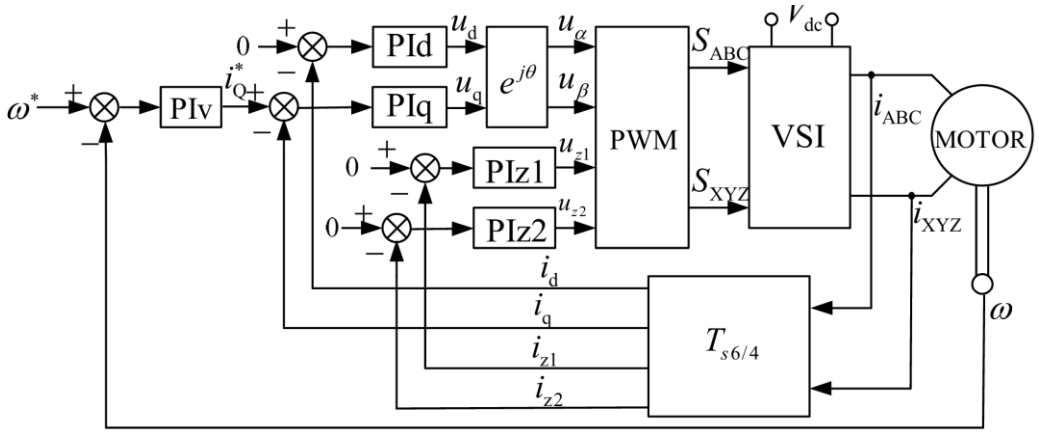

Figure 35 - Rotor field-oriented control of six-phase PMSM (3.1.)

This naive control methodology is based on the principle that in the DQ vector representation, only the current fed into the q-axis generates a mechanical torque. The resulting control achieves good performance but requires a greater rms current quantity. Current is set zero in the d, z1, z2 axis but a small quantity normally flows producing losses. So that method is unsophisticated with respect to the MTPA concept. This first control was used in the debugging phase of the system because it guaranteed an almost 1:1 ratio between the measured torque graph and current in q, so it was possible to understand how the PI regulators reacted to the required reference and to find any differences in the transients in the various plots under study.

3.1.2. MTPA based control

Maximum Torque per Ampere (MTPA) is a control strategy used to achieve the highest possible torque for a given current, optimizing efficiency and reducing losses. This is particularly beneficial in applications such as electric vehicles, where there is the need for better torque tracking for any speed condition.

The torque equation for an IPM motor is:

$$T_e = \frac{3}{2} p\left[\lambda_{pm} i_q + \left(\mathrm{L}_d - L_q\right) i_d i_q\right]$$

MTPA control seeks to find the optimal relationship between i_q and i_d to maximize torque for a given stator current *I*

$$I = \sqrt{i_d^2 + i_q^2}$$

The optimal d-axis and q-axis current relationship can be derived from torque maximization and is expressed as:

$$i_d = -\frac{\lambda_{pm}}{2(L_d - L_q)} + \sqrt{\left(\frac{\lambda_{pm}}{2(L_d - L_q)}\right)^2 + \frac{I^2}{L_d - L_q}}$$

This equation determines i_d as a function of *I* given the machine parameters. These calculations have already been carried out for each speed through simulations in Ansys Motor-CAD. Using the efficiency maps, the LUTs on which to base the MTPA control were derived.

Operationally, the LUTs have been placed in the outer loop that handles the transformation from required torque to required current in axes D, Q, Z1, Z2

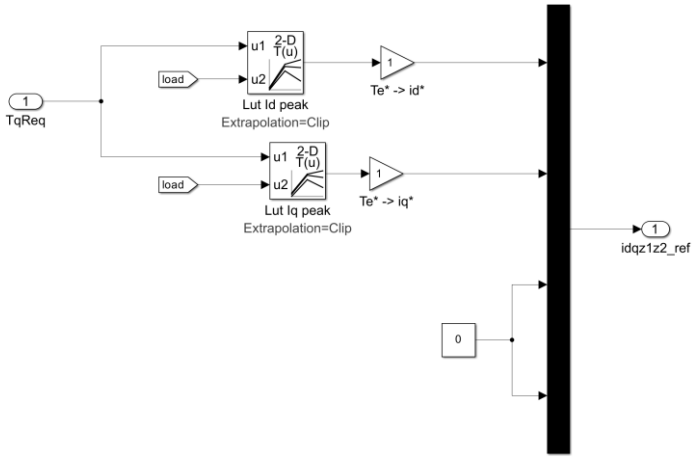

Figure 36 - Outer loop

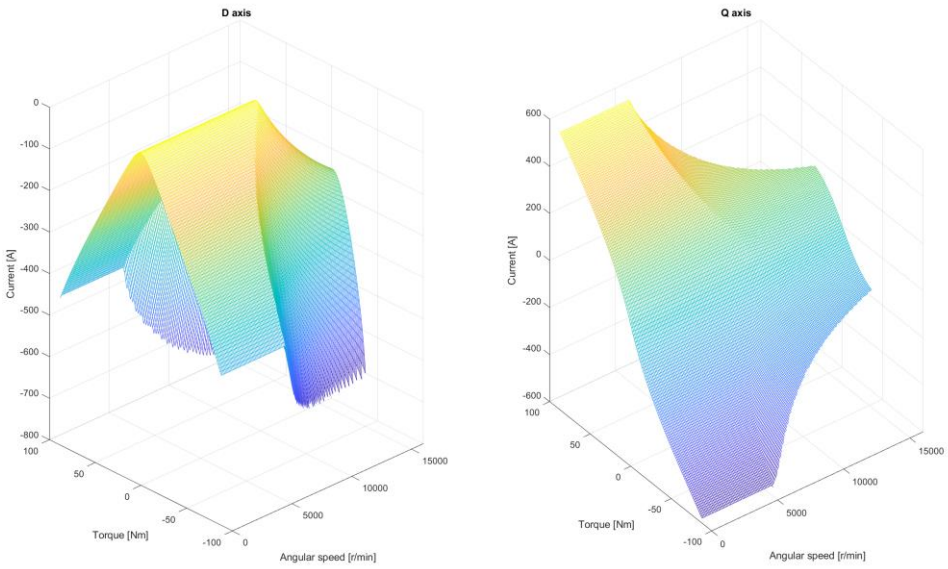

Figure 37 - LUT for MTPA

3.2. PI tuning

In the scheme below is showed the block representation of system transfer function:

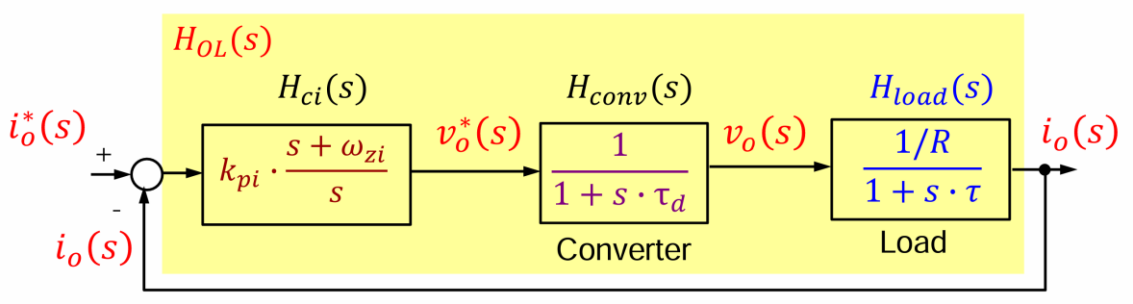

Figure 38 - Controlled PI system

The motor is described as a simple RL load, the converter behaves as a delay with a pole in $\tau_d = 1.5 \cdot T_{sw}$. The $H_{ci}(s)$ is the PI regulator transfer function.

The tuning of PI follows an open loop fashion, and it's based on the $H_{OL}(s)$ computation. The general idea it's to choose the poles of $H_{ci}(s)$ to cancel the dynamic of $H_{load}(s)$.

$$H_{OL}(s) = K_{pi} \cdot \frac{s + w_{zi}}{s} \cdot \frac{1}{1 + s \cdot \tau_d} \cdot \frac{1/R_s}{1 + s \cdot \tau}$$

With: $w_{zi} = \frac{K_{ii}}{K_{pi}}$

Imposing for the three different controllers, to obtain the zero-pole cancellation:

$$w_{ziLd} = \frac{Rs}{Ld} \quad w_{ziLq} = \frac{Rs}{Lq} \quad w_{ziL0} = \frac{Rs}{L0}$$

We obtain:

$$H_{OL}(s) = K_{pi} \cdot \frac{1}{1 + s \cdot \tau_d}$$

Approximating the crossover frequency: $|H_{OL}(jw)|_{dB} = 1 \rightarrow w_{ci} \cong \frac{K_{pi}}{L}$

We can find the values of K_{pi} knowing the maximum crossover frequency is limited by the converter dynamic, imposed by $\tau_d = 1.5 \cdot T_s$

$$w_{ci,max} = \frac{1}{\tau_d} = \frac{1}{1.5 \cdot T_{sw}} = \frac{f_s}{1.5} = 2 \cdot \pi \cdot f_{ci,max} \ (rad/s)$$

The crossover frequency is limited at about one tenth of switching frequency.

$$f_{ci} = f_{ci,max} \approx \frac{f_{sw}}{10}$$

Then

$$K_{ii} = K_{pi} \cdot w_{zi} \ (V/As).$$

So direct formulas for controller are:

Proportional gain D controller	$K_{pi_d} = 2 \cdot \pi \cdot f_{ci} \cdot L_d$
Integrator gain D controller	$K_{ii_d} = K_{pi_d} \cdot w_{ziLd}$
Proportional gain Q controller	$K_{pi_q} = 2 \cdot \pi \cdot f_{ci} \cdot L_q$
Integrator gain Q controller	$K_{ii_q} = K_{pi_q} \cdot w_{ziLq}$
Proportional gain Z1 and Z2 controllers	$K_{pi_0} = 2 \cdot \pi \cdot f_{ci} \cdot L_0$
Integrator gain Z1 and Z2 controllers	$K_{ii_0} = K_{pi_0} \cdot w_{ziL0}$

wzi (L_d)	57.1313
wzi (L_q)	23.5419
wzi (L_{012})	122.6509

Table 3 - Natural frequency for PI controllers

Using the values proper of the motor reported on Table 5 - Motor Parameter the following diagram bode showing the $H_{OL}(jw)$ and $H_{CL}(s)$ magnitude and phase parameters.

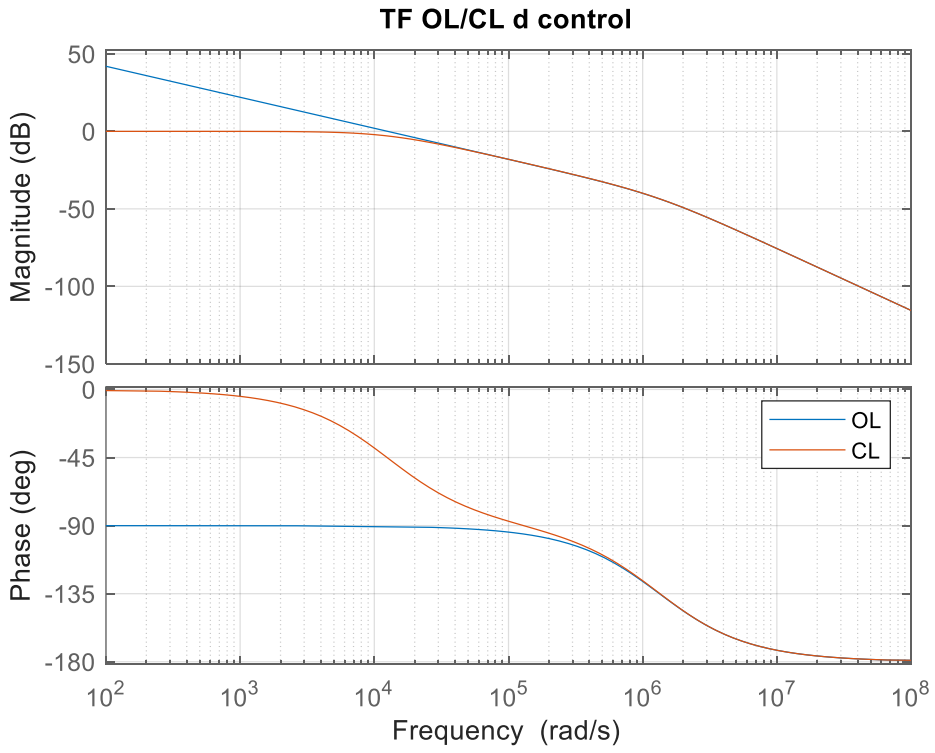

Figure 39 - D axis control TFs

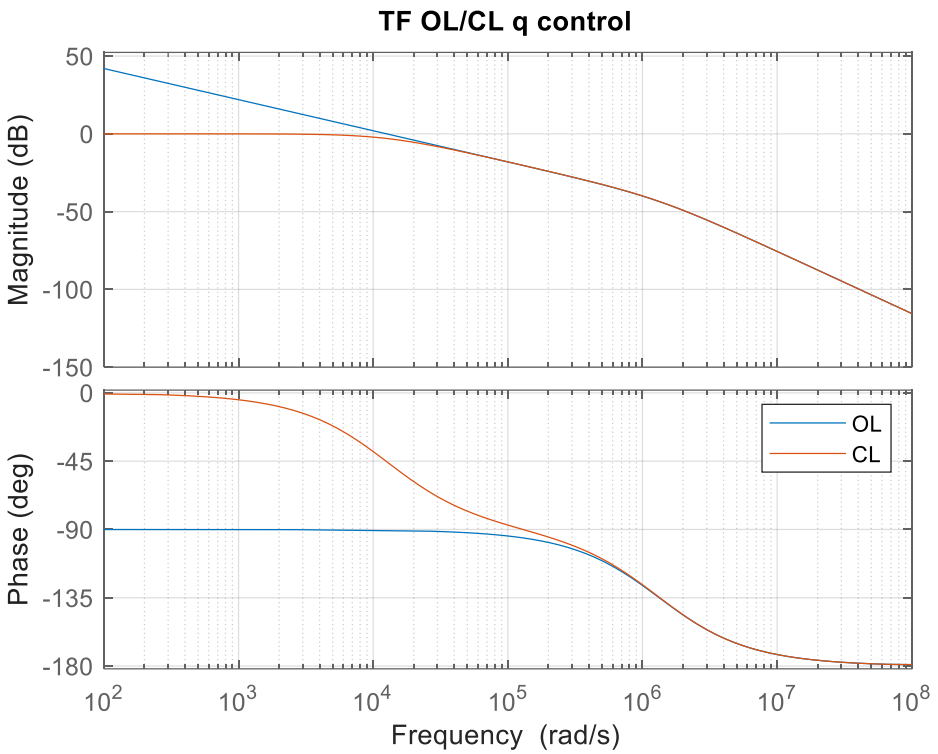

Figure 40 - Q axis control TFs

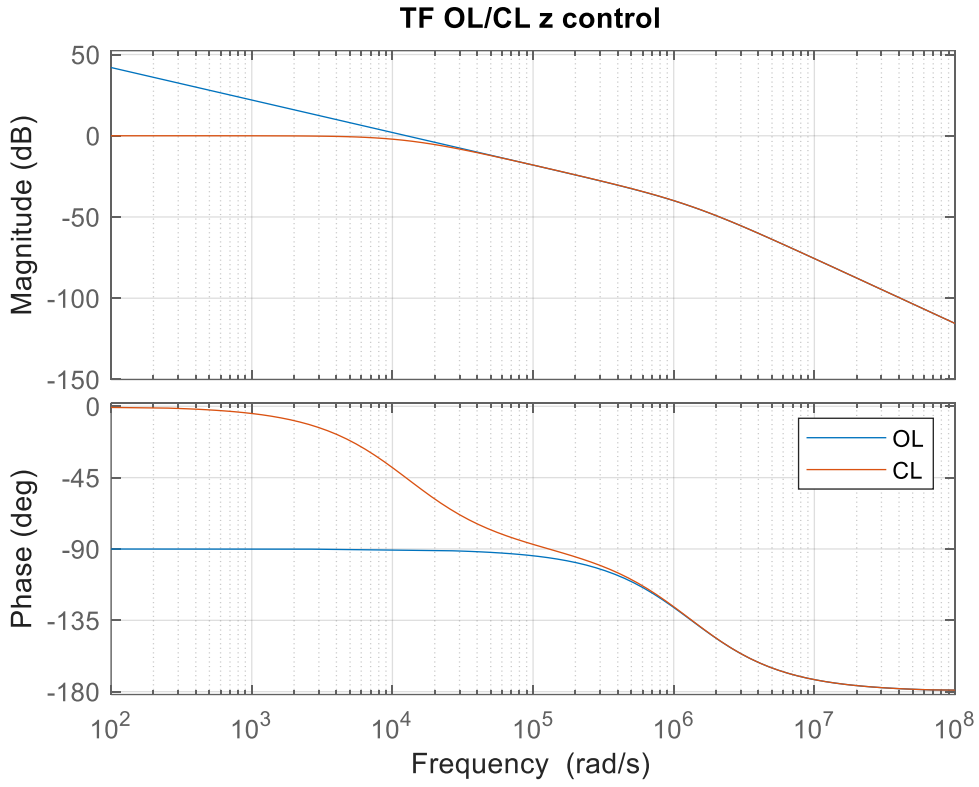

Figure 41 - Z1 an Z2 axis control TFs

Analysis of the bode diagram demonstrates zero-pole cancellation for all three controllers. This means that the influence of the different inductances is eliminated. Continuing to analyze the open loop function we have a slope of -20 dB per decade up to the frequency of $1.333 \cdot 10\text{^}6$ (rad/s) where is placed the characteristic pole imposed by τ_d. The phase margin is very high $\Phi = 89.4600$, which is a very good parameter because it gives the system great stability. Crossover frequency set at $1.2566 \cdot 10\text{^}4$.

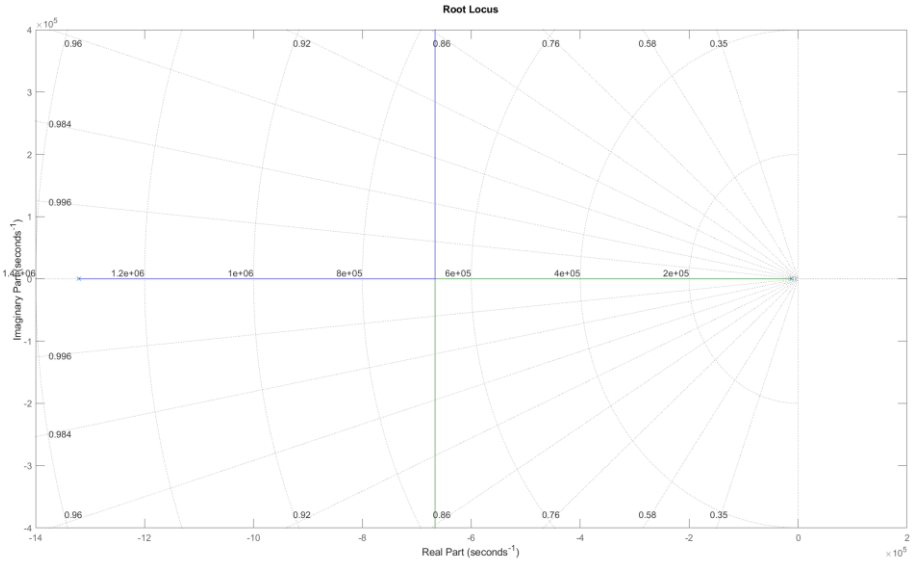

Figure 42 - Roots Map closed loop function

The closed-loop poles are placed in $-1.3206 \cdot 10^6$ and $-0.0127 \cdot 10^6$

3.3. Simulation setup and settings

Here are the tables with the parameters used for the characterisation of the blocks in the Simulink structure:

Sampling Times and Frequency			
Ts	$5 \cdot 10^{-7}$	s	Fundamental sample time
Tsc	$5 \cdot 10^{-5}$	s	Inner control block period
fsw	20000	Hz	Switching frequency
fci	2000	Hz	Bandwidth frequency

Table 4 - Sampling times and frequency

The fundamental sampling time was chosen with two orders of magnitude in relation to the swirling time to be able to track the dynamics of the output quantities the sampling block with great precision. The choice of these values stems from the rated values of the hardware components that should implement the design, so the switching speed of the inverter and the processing speed of the microcontroller were taken into account as limiting parameters.

Motor Parameter			
p	4		Pole pairs number
Vdc	52	V	Rated voltage
Rs	$6.3987 \cdot 10^{-4}$	Ohm	Stator resistance phase
Ld	$0.0112 \cdot 10^{-3}$	H	Stator d-axis inductance
Lq	$0.02718 \cdot 10^{-3}$	H	Stator q-axis inductance
L0	$0.005217 \cdot 10^{-3}$	H	Stator leakage inductance
λm	0.0073	Wb	Permanent magnet flux linkage
Jm	0.0088734	$Kg \cdot m^2$	Rotor Inertia

Table 5 - Motor Parameter

To make the control efficient and validate the action of all the blocks involved in the structure, several simulations were carried out. The simulations were repeated by varying the control between the strategy of only varying in the Q-axis and using LUTs. The selection on the DQ limiter was tested with the three possible options: "prioritize d," "prioritize q," and "dq balance." In all cases, the limiter acted positively, filtering the voltage peaks generated; however, better performance was achieved when the selection was set to "prioritize q" in terms of overshoot limitation during step changes in the d-axis current demand. Nonetheless, in some cases, prioritizing q slowed the tracking on increasing torque ramps, leading to the decision to conduct all proposed tests using the "dq balance" option. This choice also aims to highlight the difference between the two control strategies under study, ensuring that the dq limiter does not alter the action of the LUTs, which, when correctly calculated, provide the best current values for the motor axes. As discussed above, the customised electric motor block better represents reality and has better tracking performance, all preliminary simulations and model validation have been carried out with the custom block. However, the model is much more complex and requires many more calculations per single simulation cycle, so it was decided to use the linear model proposed in the standard MATLAB libraries for the long simulations. According to the estimates made, the simulation time is shortened by 4-6 times, which becomes of fundamental importance for the simulation of drive cycles involving several hours of simulation. Finally, it is important to clarify, the custom block uses flow data calculated at a certain operating rpm. Having been characterised at a low rpm operating point, it was noted that it is not possible to simulate correctly at speeds much higher than the speed reference set in Motor-cad to extrapolate the data, so the use of the standard MATLAB block was again preferred in simulations where there is a large variance in speed.

In the light of the considerations made, the following types of simulations are proposed in this work to visualise the performance of the control and more generally to be able to formulate conclusions on the system thus structured:

- Constant speed and torque variation to evaluate the error with respect to the reference without the disturbances due to rotational variation.
- Constant torque and speed ramp, this test is very important for assessing the stability of the system over long simulations and exploring its limits.
- Drive cycles, useful for stressing the system with characteristic references in real application fields
- Simulations with unbalanced Vdc bus, to test the maximum tolerance levels on the control before failing

4. Simulation results

In this chapter, the graphs and numerical values from the proposed simulations will be analyzed. Some preliminary considerations regarding the simulation settings will be made before analyzing in detail the test in question. The study of the results has played a key role in the project as it determines which elements need to be focused on for the validation and improvement of the project.

4.1. Constant speed

In this test, the reference signal consists of a series of increasing and decreasing steps. This is one of the first simulations performed. However, it is fundamental for the qualitative analysis of the model. By maintaining the load at a constant speed, it is possible to analyze the torque response the system can achieve and identify any disturbances it suffers from, without being affected by the transients that cannot be neglected in the motor's voltage equations.

SETTINGS:

- 1500 RPM constant value
- DQ limiter in balance mode
- MTPA LUT
- Custom motor Simscape block

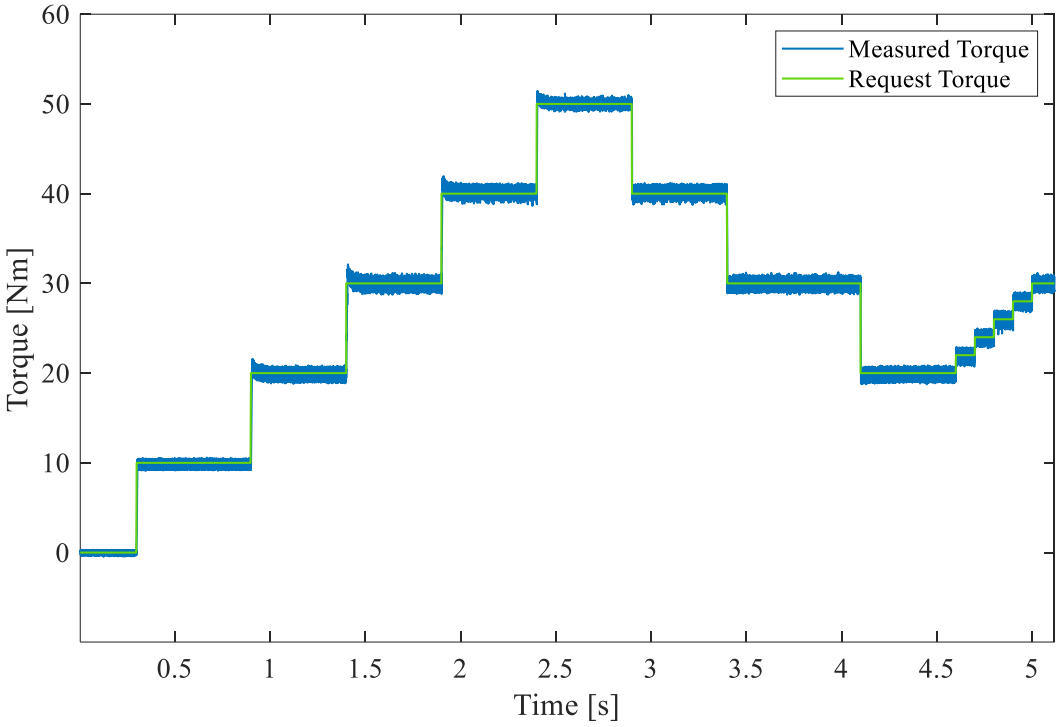

Figure 43 - Reference and Measure Torque

Analysing the graph of measured torque vs required torque, a very good tracking result can be seen. The system has some overshoot in the presence of large steps, but the settling time is satisfactory. Looking at the first simulation instants, it is possible to calculate the cogging torque, which turns out to be about 0.28 Nm (rms value). In the following seconds, however, the torque ripple remains low and constant with a value of approximately 3 Nm peak-to-peak and zero mean value.

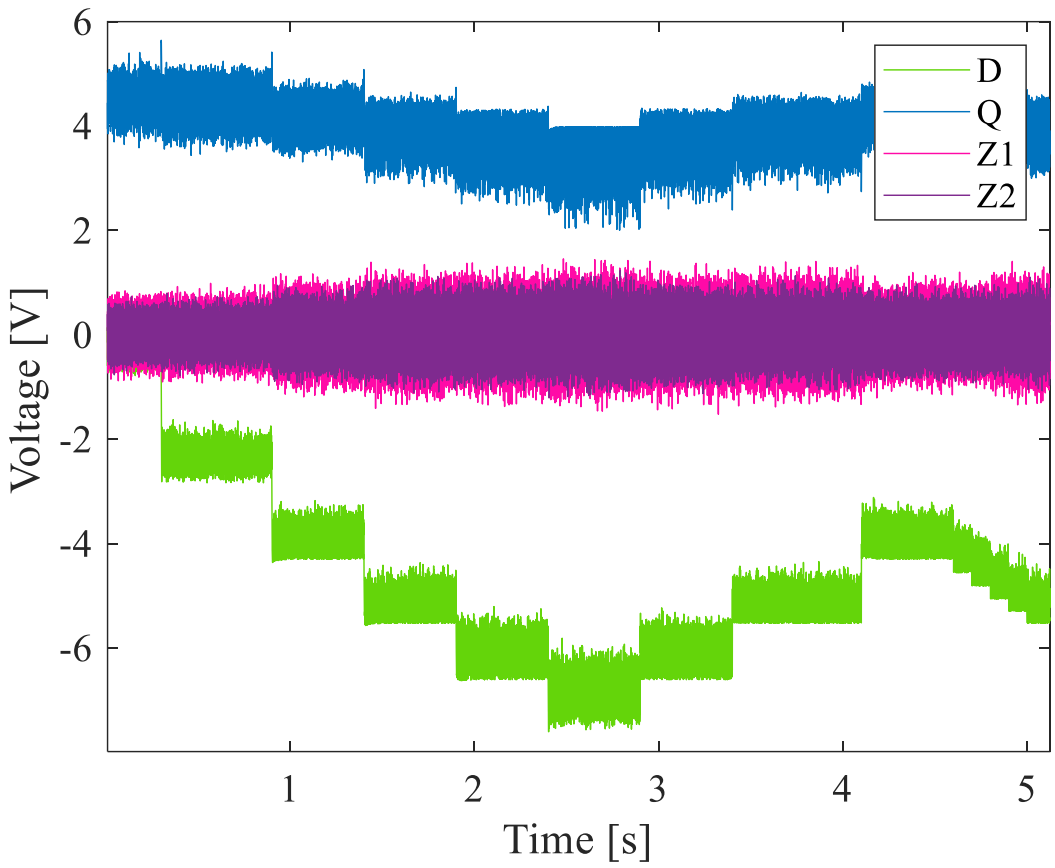

Figure 44 - Voltage D Q Z1 Z2

Looking at the voltages in DQ axis, it is possible to see how control is crucial to contain the variation imposed by the load. As the required torque increases, the voltage that is dissipated in Z1 and Z2 increases, limiting the possibility of greater system dynamism. It is possible to see how the voltage in Q is saturated above the torque step of 50 Nm.

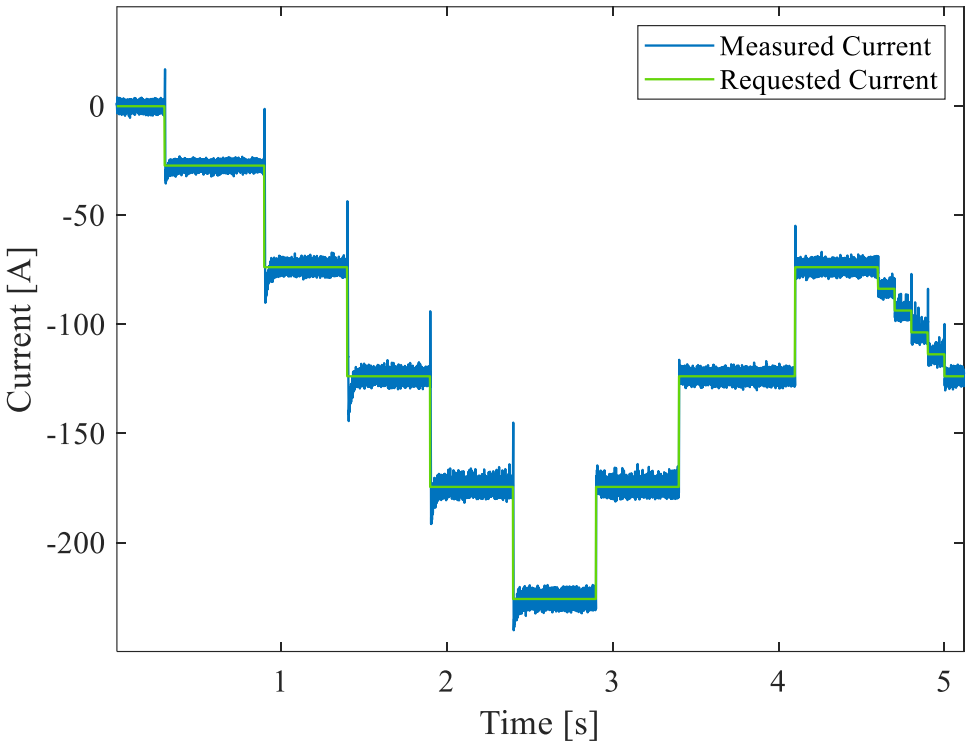

Figure 45 - Reference and measured D - axis current

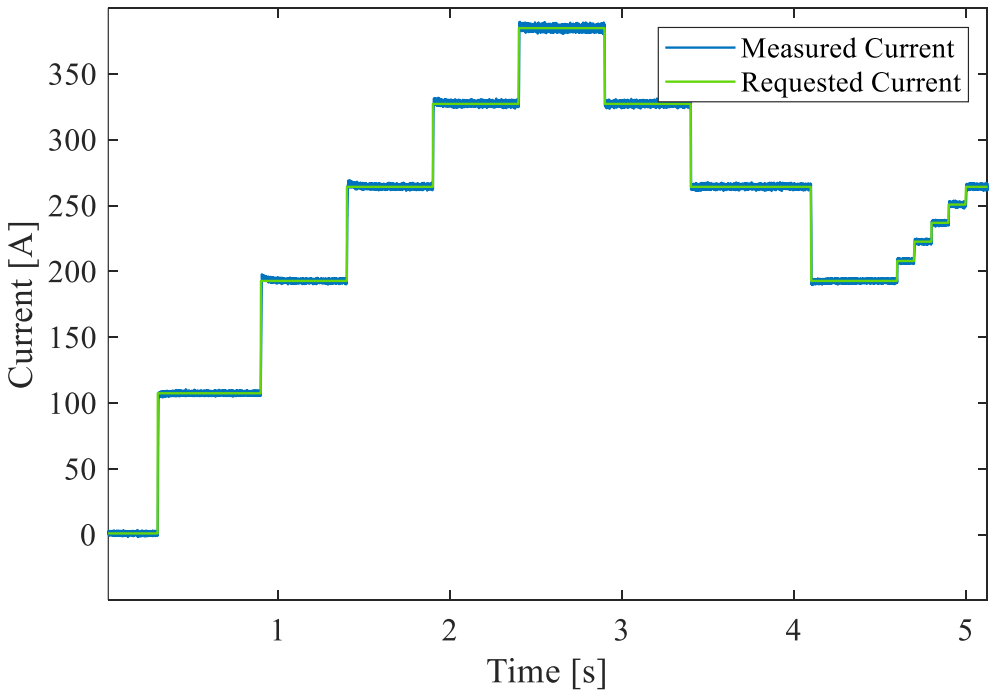

Figure 46 - Reference and measured Q - axis current

The calculated current measured in the Q-axis exhibits very good behavior compared to the ideal, with a current ripple which, although increasing as the required value rises, is

negligible for the purposes of quality assessment. The current in the D-axis has similar behavior and the considerations made above can be extended, however, there are noticeable peaks at increasing torque steps. A possible explanation for this effect can be attributed to an offset or inaccuracy of the LUTs. After several simulations it was found that the effect can be mitigated, in fact by changing the setting of the DQ limiter, by prioritizing Q, the D-axis undergoes greater saturation. However, this choice results in a larger settling time in the required torque tracking.

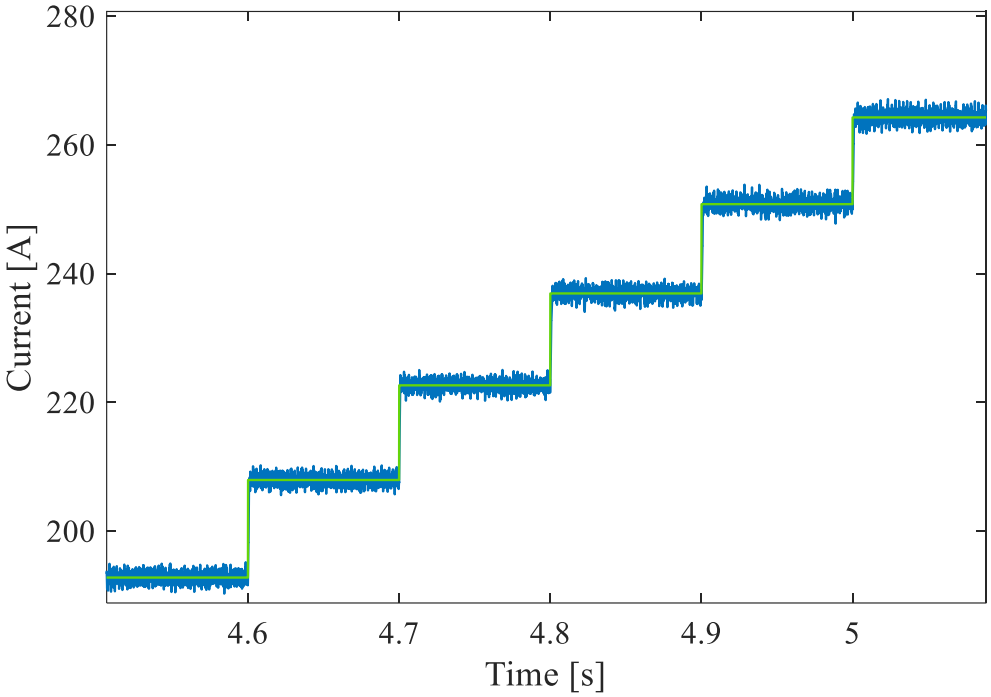

Figure 47 - Zoom on Q -axis current graph

Below are the current graphs represented in the ABC model:

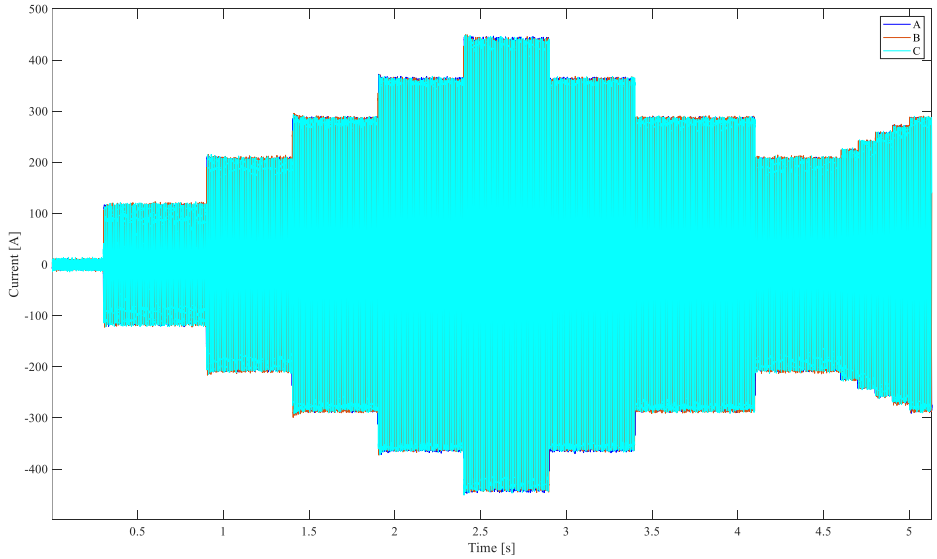

Figure 48 - Measured ABC current

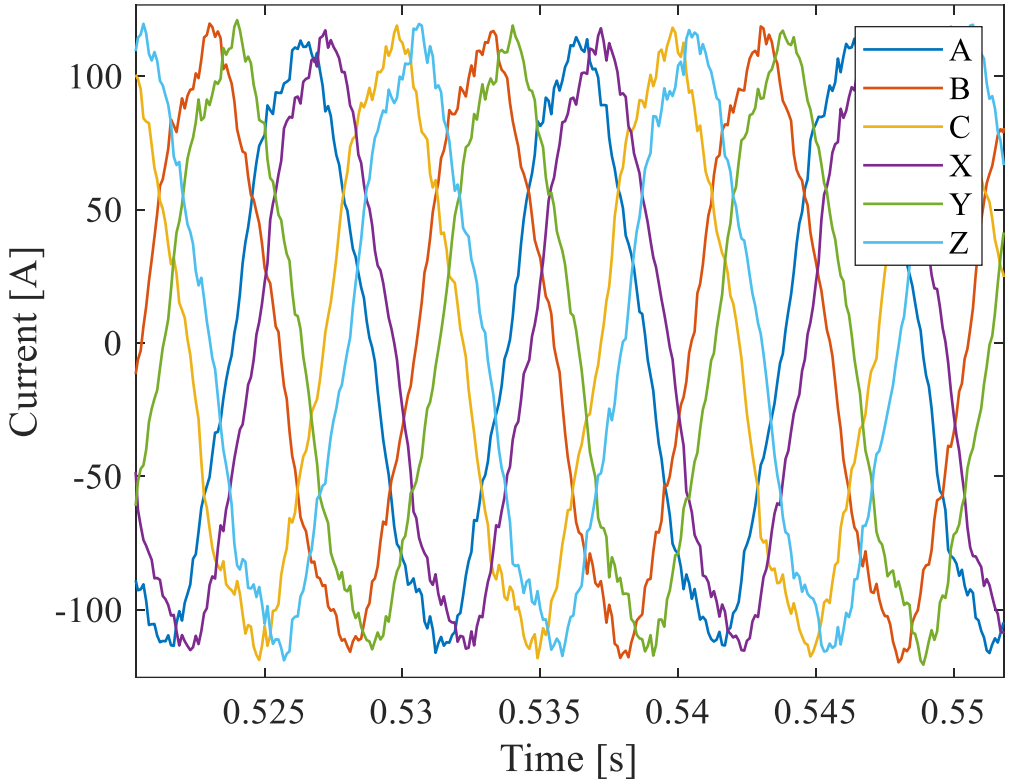

Figure 49 - ABCXYZ current component

The measured quantities are the output values of the individual motor phases. The sinusoidal form is respected, but distortions due to the harmonic content can be seen that the model can handle. The study of these distortions with respect to ideality is the next step in refining the control, through the suppression of these disturbances introduced by the geometry of the electric motor.

4.2. Constant Torque

In this test, a constant torque value is set, and the rotational speed starts from zero and increases linearly. The theoretical result predicted for this simulation is an increase in frequency in the sinusoidal currents, the system should be able to produce the required torque for each imposed rotational speed value.

SETTINGS:

- Torque: 35 Nm constant value
- Linear RPM increase from 1000 to 2500
- DQ limiter in balance mode
- MTPA LUT
- Custom motor Simscape block

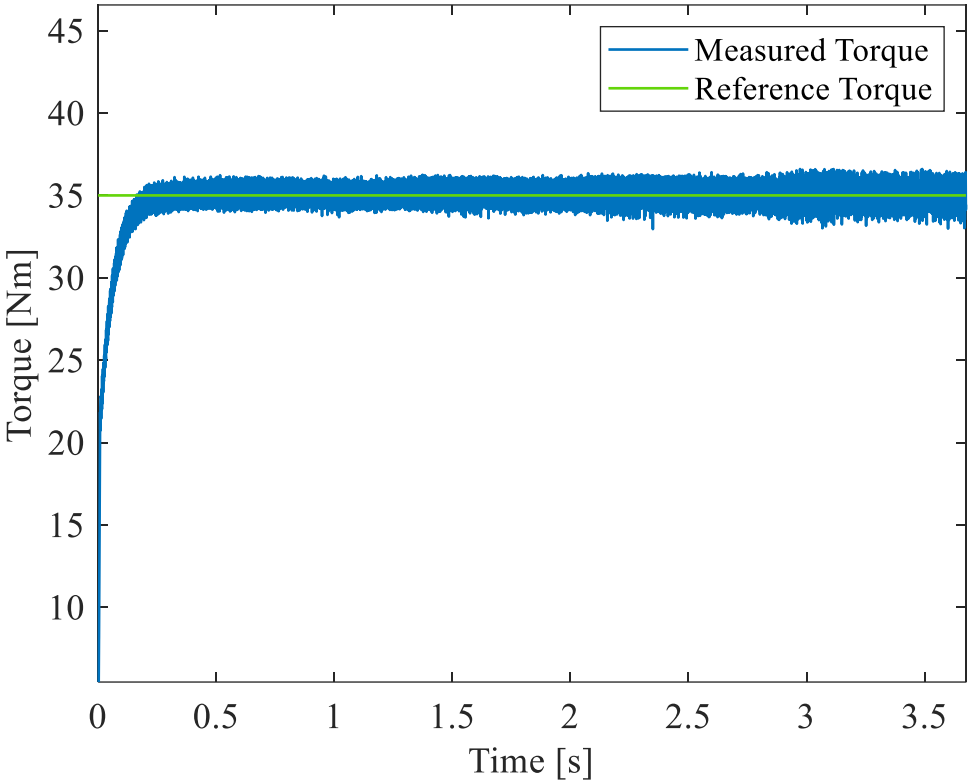

Figure 50 - Refence and measured torque

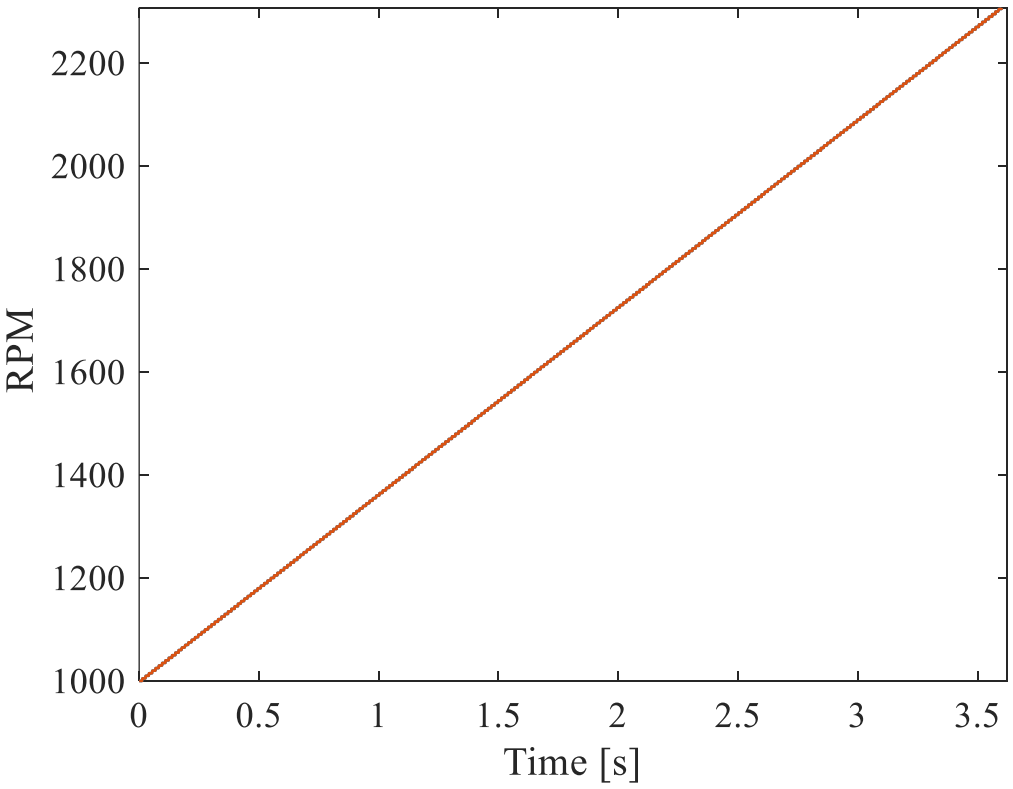

Figure 51 - Reference RPM load

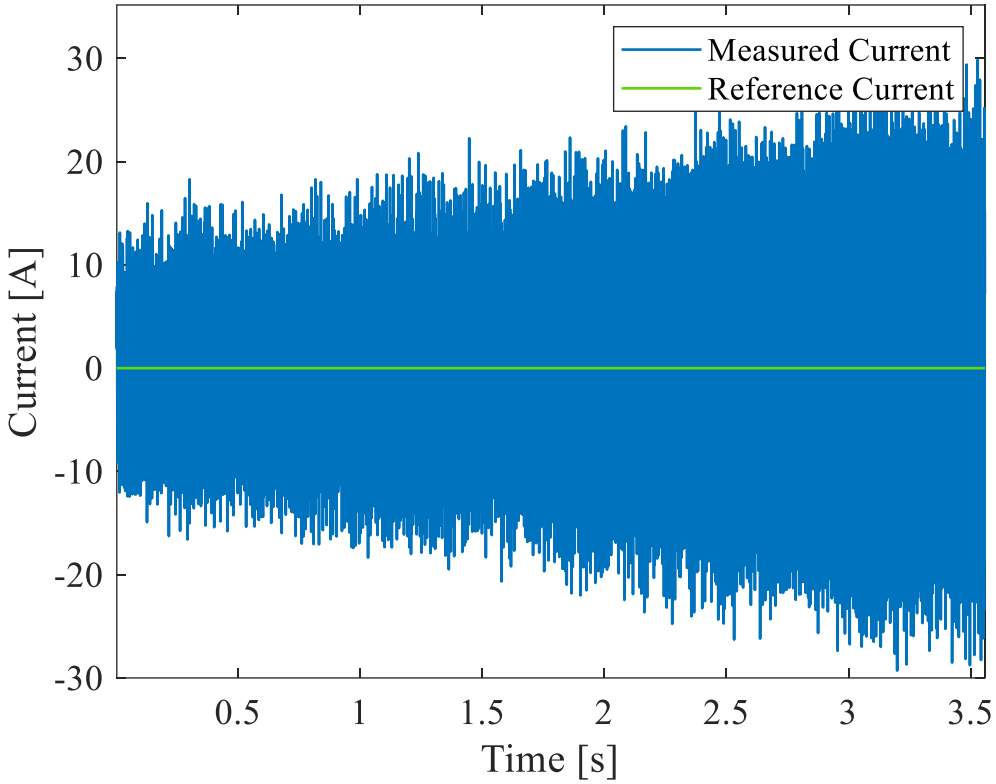

Figure 52 - Z1 current

Reading the graphs, one notices the excellent rising time of about 0.25 seconds for a delta of 35 Nm. The average torque value remains constant and consistent with the required reference throughout the simulation time. However, the average ripple amplitude tends to increase with increasing angular speed. Once again, the analysis of currents in z1 and z2 is of paramount importance. In fact, the currents in q and d are unaffected by speed variation, whereas the current in z1 tends to increase with the same variation as the measured torque. A possible suppression of the current in z1 and z2 could improve efficiency in terms of saving energy consumed and reducing the vibrations produced by the motor.

4.3. Urban Drive Cycle

In this simulation, a portion of the drive cycle of about 15 seconds is proposed, which was used to extract the operating points of the motor, with the aim of optimising the design of the electric machine to be performance-oriented at the operating points collected. In particular, the drive-cycle refers to an urban scenario, whereby the motor will always operate at relatively low speeds in terms of angular velocity. Differently, the torque demand undergoes large variations in a short time, reproducing the rapid accelerations a vehicle must perform in traffic or after an intersection. Simulation of portions of the drive cycle plays an important role in the project because it is a preliminary validation prior to hardware testing.

In the proposed simulation, an almost constant positive change in rotational speed is made, while torque rises and falls in steps that are not constant in amplitude. As already explained in the previous chapter, for computational speed in the simulations, it was decided to simulate with the MATLAB linear model. The validity of the simulation results is therefore to be understood more qualitatively on the ability of the control in tracking the required references and handling transients, rather than on the analysis of numerical values in the strict sense.

SETTINGS:

- RPM variable
- Torque variable
- DQ limiter in balance mode
- MTPA LUT
- Six phase PMSM block

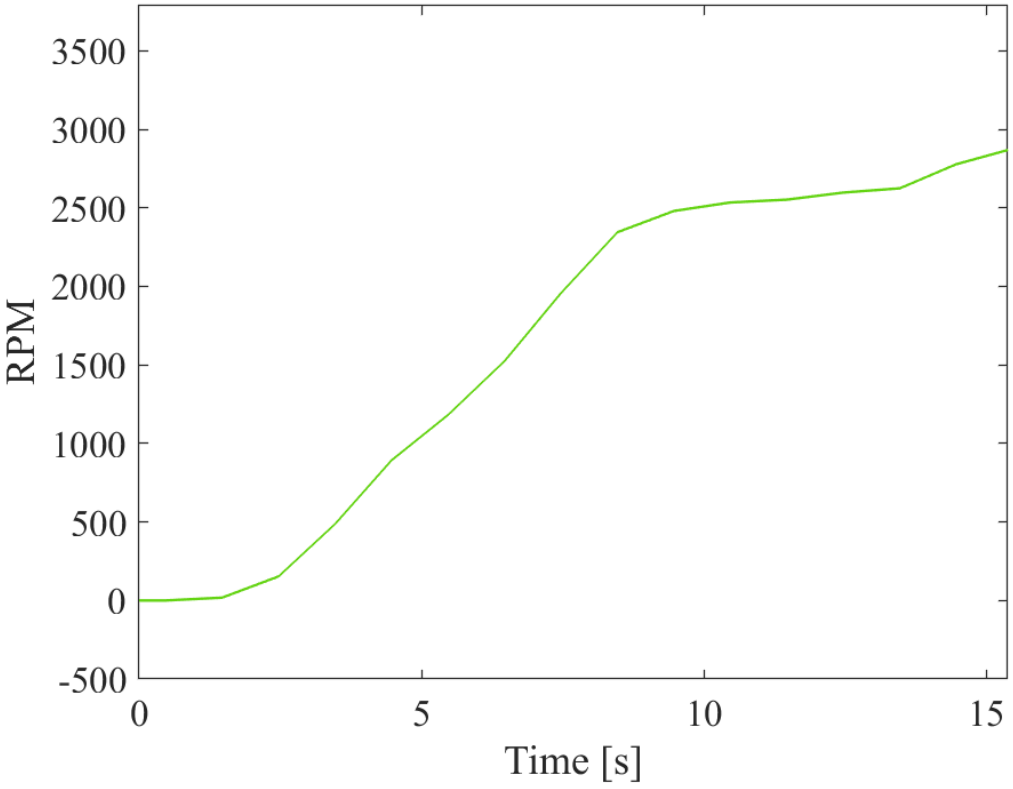

Figure 53 - Speed profile

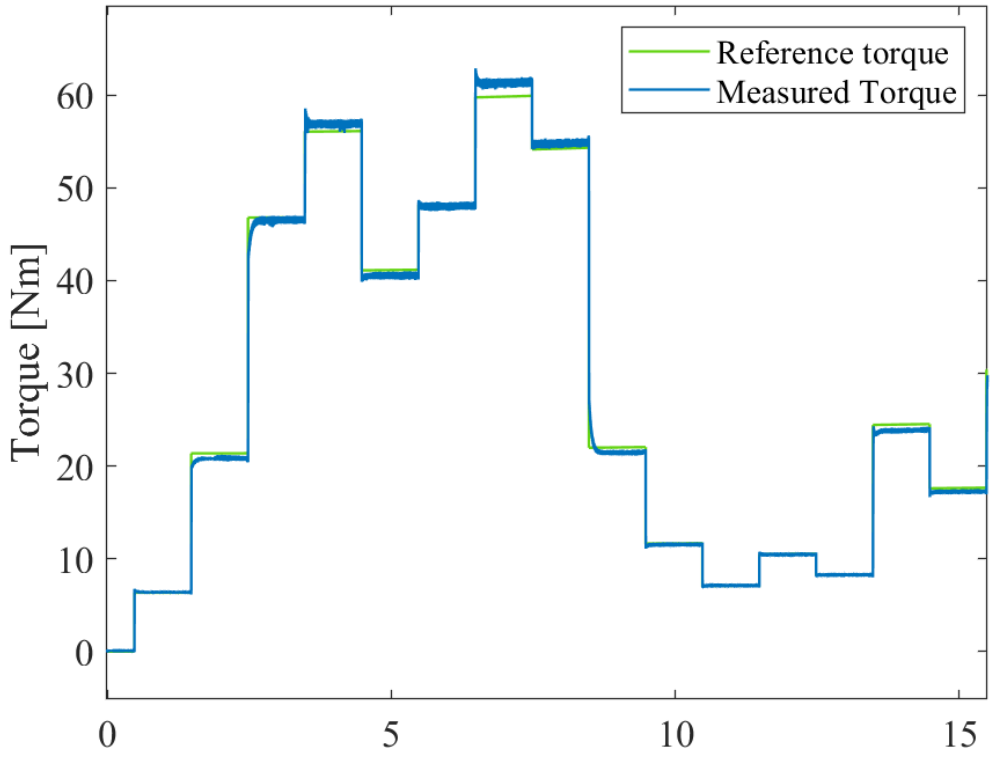

Figure 54 - Refence and Measured Torque

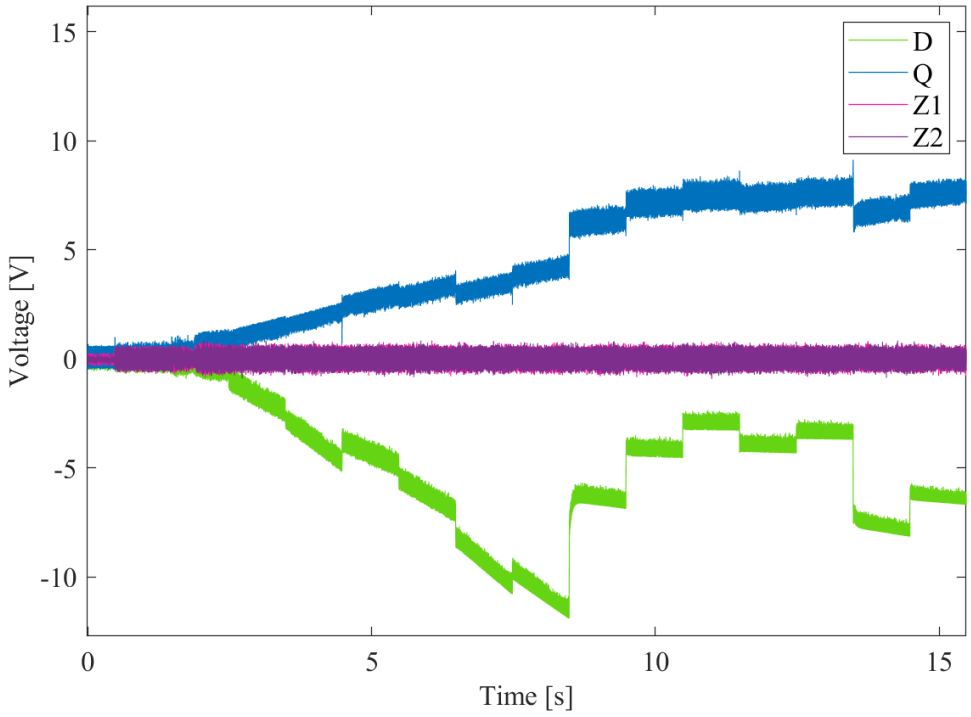

Figure 55 - Voltage D Q Z1 Z2

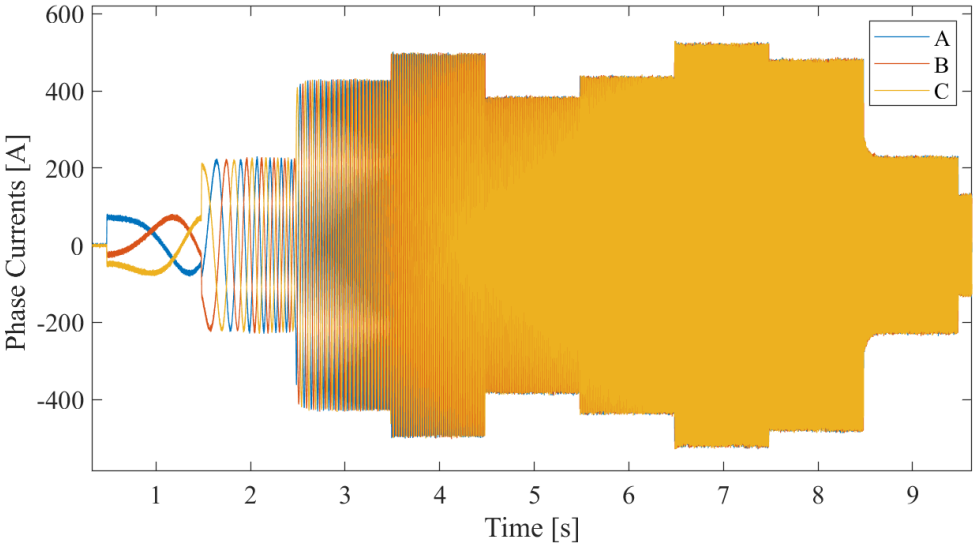

Figure 56 - ABC current

The results still appear to be consistent with each other and with previous simulation. Analyzing the measured torque graph, it is possible to see how there are some offsets of a few Nm in correspondence with large steps. This effect is attributable to the LUTs that were obtained from the much more complex model in Ansys Motor-CAD, and combined with the more linear model, producing some alteration compared to the custom block. The torque tracking except for the offsets already discussed is satisfactory. Other details that can be noted are that in case of variations of about 10 Nm the system has an evolution of a second order system with an overshoot sometimes even important, but that extinguishes very quickly. For steps greater than or equal to 15 Nm, the system enters saturation and needs a larger rising time. However, the settling time in both cases is comparable. Finally, torque tracking is not affected by load variation in rotational speed. Looking at the voltage graph, it is immediately noticeable that the voltages in Z1 and Z2 remain constant as the speed and torque produced vary. This is one of the main differences between the two blocks used to simulate, in fact we would have expected an increase in the amplitudes. In fact, as already explained, being able to measure and control these two components efficiently can be the turning point for an optimized and finely tuned control on the electric motor, compared to what has already been done.

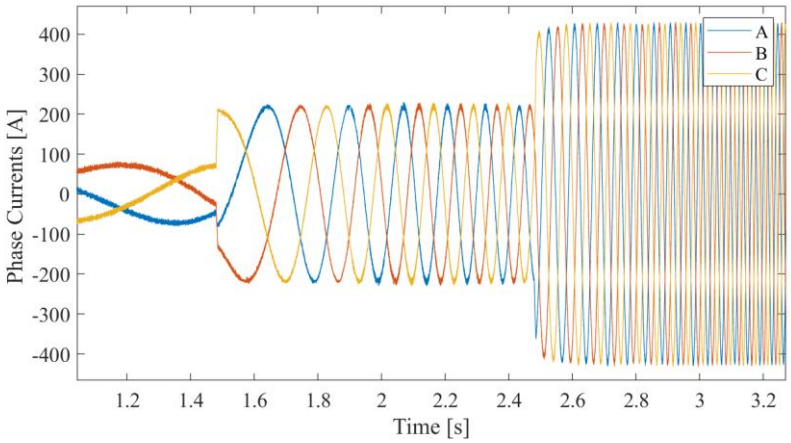

Figure 57 - zoom ABC current

4.4. Unbalanced DC bus

In this part of the chapter a different system configuration is explored. The structure in Simulink has been modified to have two separate DC bus sources, also adapting some sections of the control to try to decouple each three-phase system from the other as much as possible. The final goal is to verify the behavior of the system in case of different power supply values for the inverters, and consequently a lower power supply for one of the two three-phases in the motor. The study of these configurations is useful to understand in which circumstances the system is still able to operate in terms of phase unbalance, and how much is the difference between a balanced and an unbalanced system. Finally, one of the objectives of the configuration is to understand how much a three-phase influences the other in case of unbalance and what are the correlations due to the mutual inductances in such a multiphase electric machine.

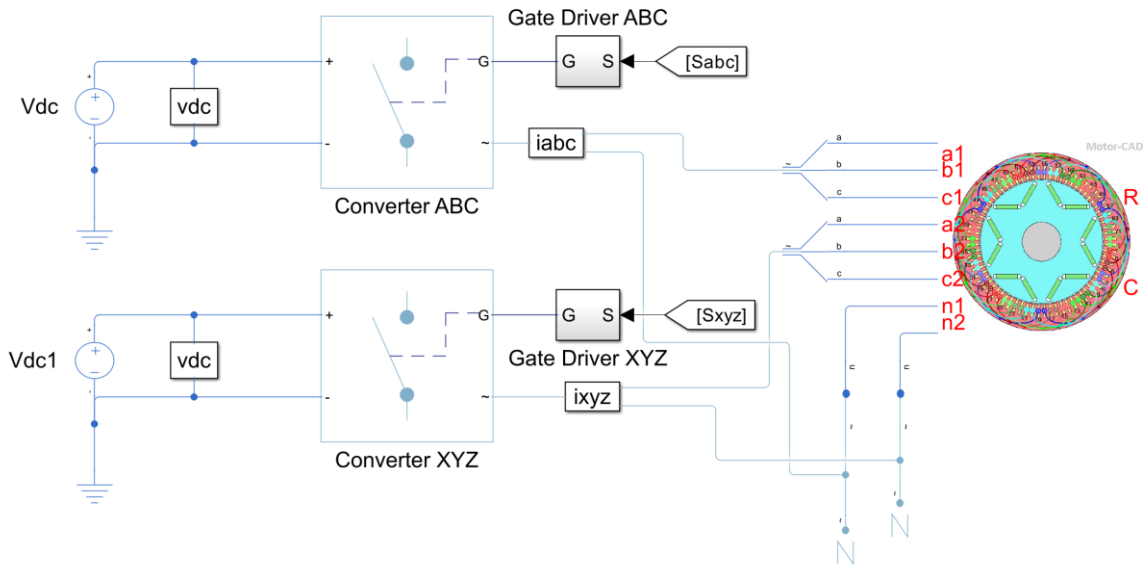

Figure 58 - Configuration for unbalanced operation

4.4.1. Unbalanced voltage 52/45 V

The first simulation carried out consists of verifying the response of the control system in the case where one inverter is powered at 52 V by default, while the other at 45 V by simulating the behaviour of a discharged battery which nevertheless still manages to supply current. The voltage difference should limit the maximum operational amplitude of the six-step vector supply. Theoretically, this should result in a lower maximum torque and a longer settling time in torque tracking dynamics.

SETTINGS:

- 1000 RPM constant
- Torque variable
- DQ limiter in balance mode
- Control on Q axis
- Custom motor Simscape block

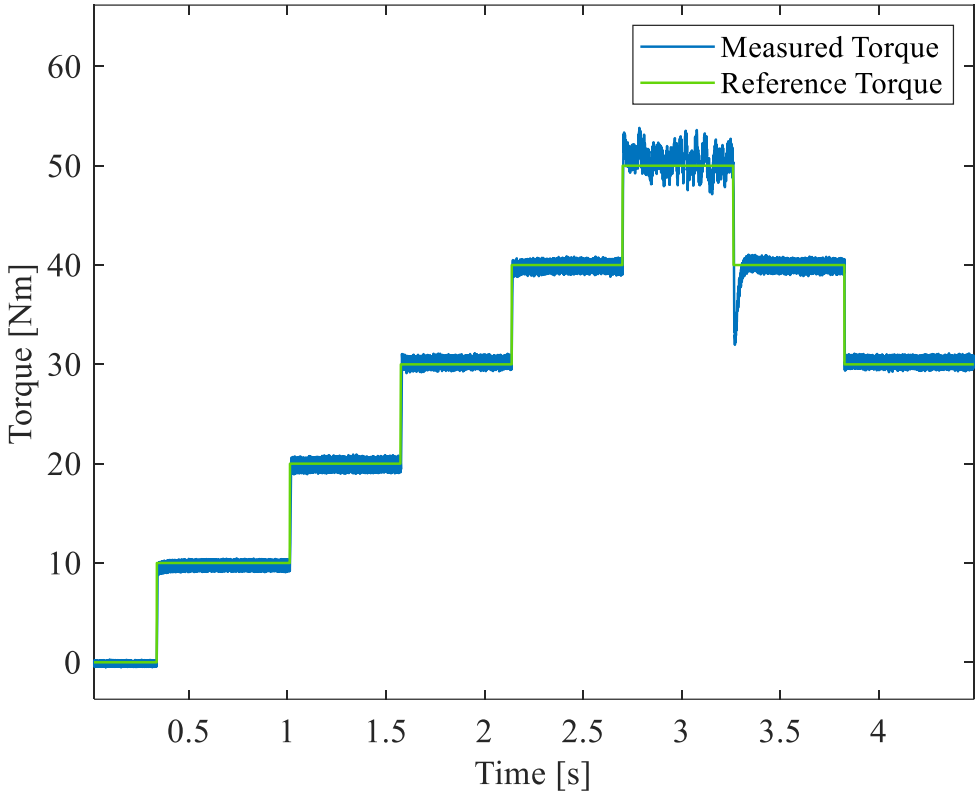

Figure 59 - Torque tracking

The measured torque graph shows that the system still manages to work correctly up to 40 Nm and is comparable with the simulation carried out previously, however, looking at the step after 50 Nm shows the control's difficulty in maintaining a constant reference, even the descending step from 50 to 40 Nm suffers from a large undershoot, a symptom that the control dynamics were already saturated.

Looking at the voltages in the DQZ1Z2 decomposition, it is evident how difficult it is for the control to handle the saturation reached. In particular, the dedicated D-axis voltage increases proportionally to the torque steps required, limiting the action of the Q-axis control above 30 Nm. The step from 40 to 50 Nm leads to complete saturation of the system, which is unable to have more voltage available from the inverters, for the control dynamics are cancelled and the torque ripples are due to the Back-EMF generated by the rotation. The voltage used in Z1 and Z2 remains stable throughout the simulation and at zero mean value as expected.

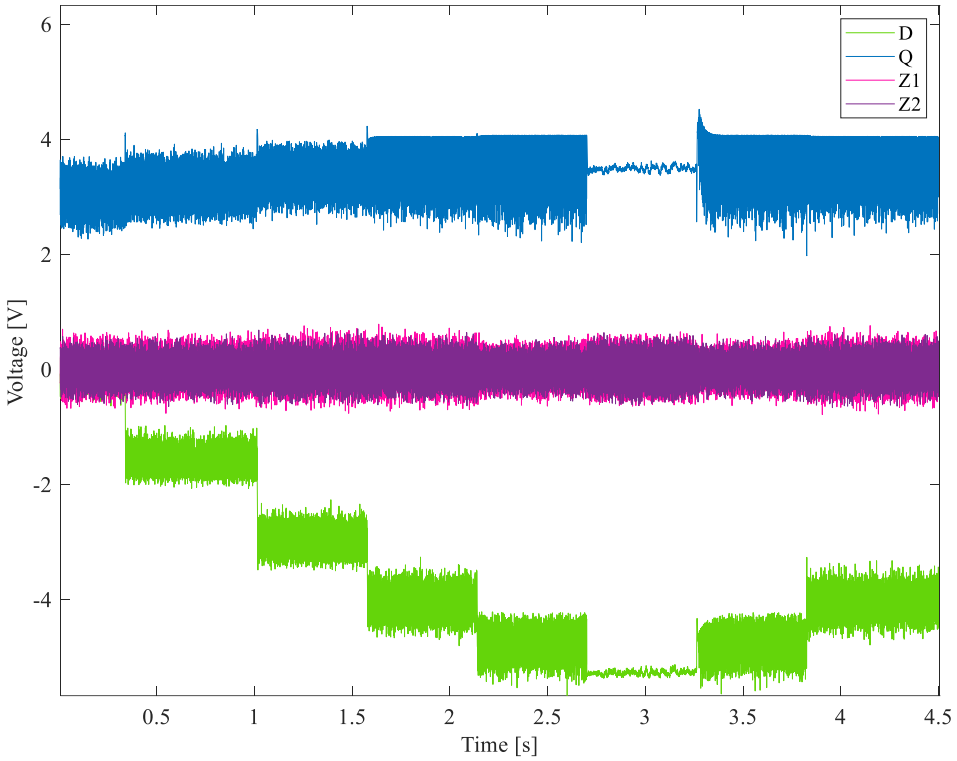

Figure 60 Voltage dqz1z2

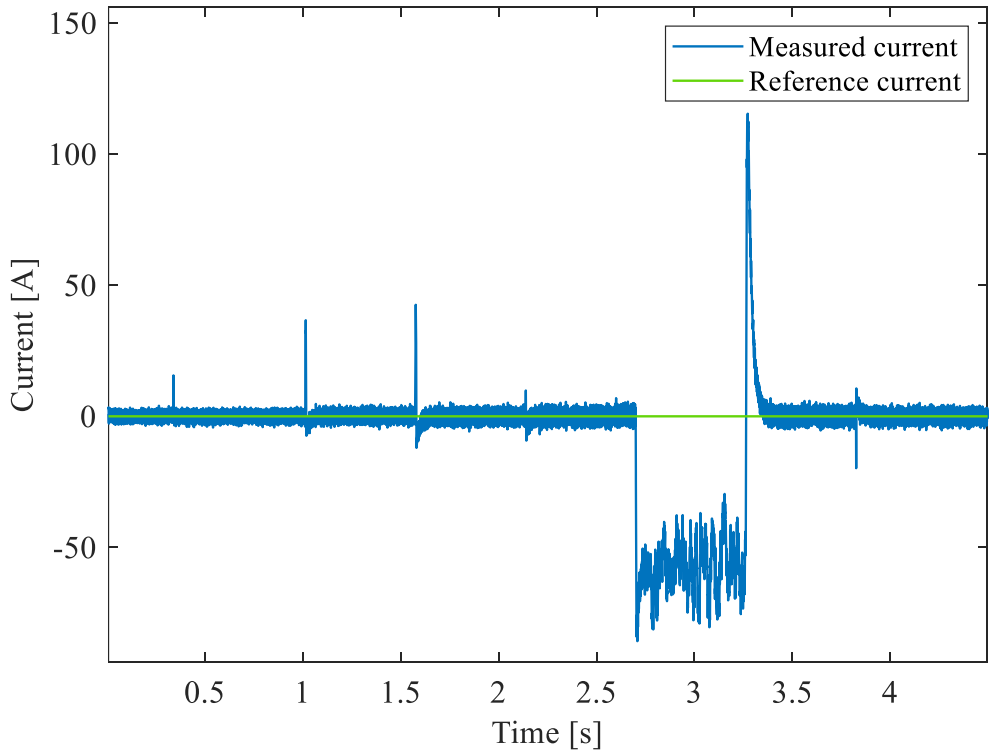

Figure 61 - D axis current

Consistent with the voltage graph, it is easy to understand the current ones. The control used constantly imposes zero current in the D-axis. When the control has saturated its dynamics, it cannot compensate for the zero-tracking demand and unwanted current is also injected in the D-axis. Large spikes are also already a symptom of a system that is not working under ideal conditions, however they are quickly compensated for until the control is saturated.

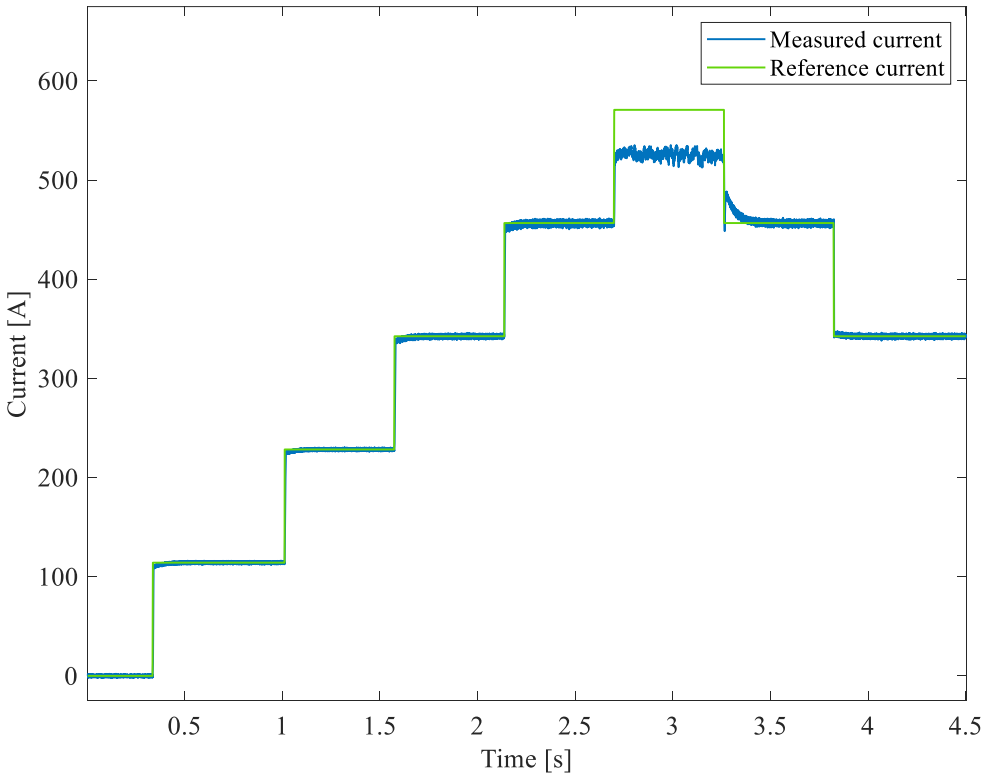

Figure 62 - Q axis current

Current tracking in Q seems to have a better response and suffers in the last step from 40 to 50 Nm from a missing current offset, which corresponds precisely to the finite current in the D-axis.

Generally, it can be stated that the system demonstrates very good robustness in a highly unbalanced operating environment that would also be extreme in application areas. The simulations therefore suggest using a logic that limits the maximum torque a user can request from the system in the event of battery malfunctions, to protect both the batteries and the motor from overcurrent and overvoltage spikes.

4.4.2. One three-phase off

The same torque and rotational speed profile of previous test was simulated, this time modifying some blocks to simulate only one inverter being turned on. To do this, a current limiter was also introduced at 0.01 A, and the voltage of the switched-off inverter was lowered to 0 V. In addition, the enable for six-step signal on the inverter was always 0. This simulation has the task of simulating a malfunction in one of the two inverters, it also aims to verify what voltages were read at the ends of the three-phase unpowered phase. In fact, since the rotational load was imposed, we wanted to verify and undertake a study on how the measured back-EMF values could be related to the behaviour of the induced currents in the non-powered phases, in order to take them into account for possible fault tolerant control.

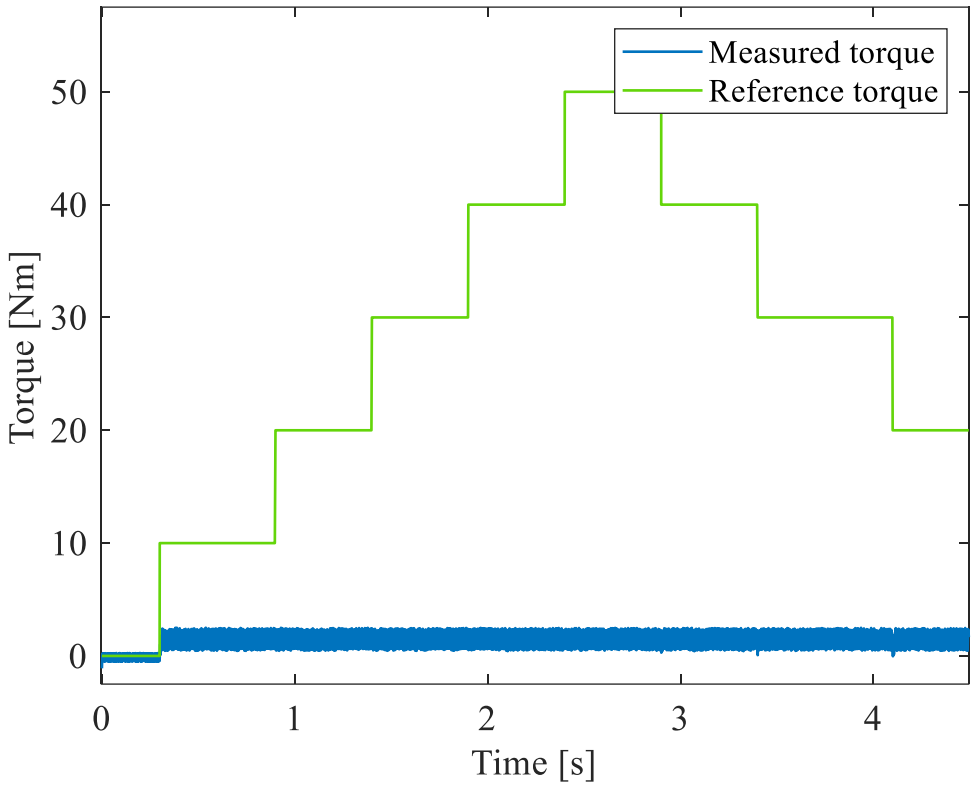

Figure 63 - Measured and reference Torque

The torque fails to follow the required reference and remains constant throughout the simulation at about 2 Nm.

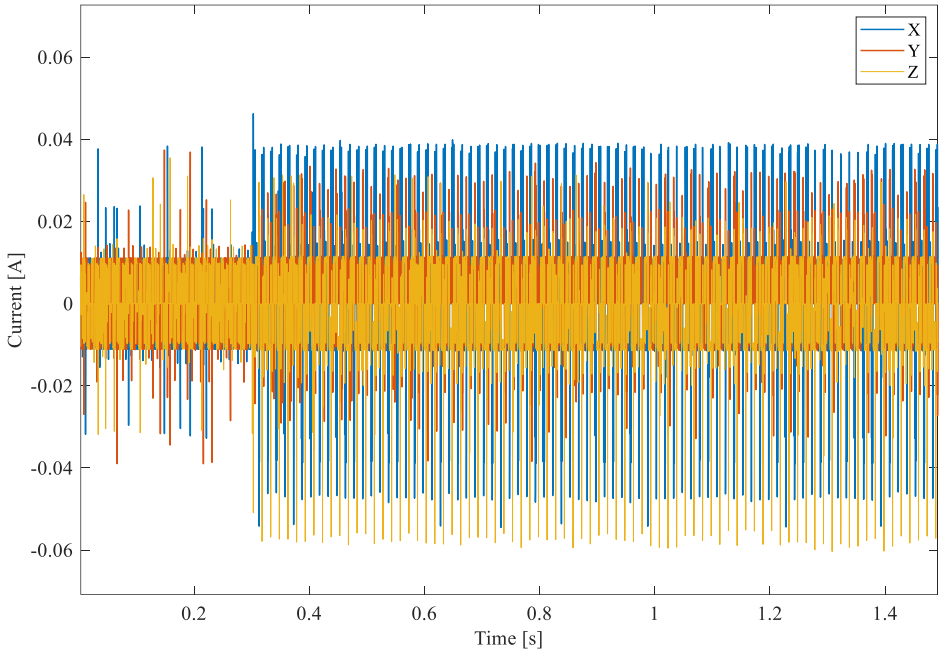

Figure 64 - XYZ current

To understand the behaviour of the electric motor in the case of a three-phase off one must look at the behaviour of the currents. It is useful to go and look at the response measured at the terminals of the three-phase off. Up to time 0.3 s the motor turn at 1000 rpm but no torque is required. The waveform consists of a main component with wave amplitude less than 0.01 A and an upper harmonic component with amplitude of about 0.02-0.04 A. As soon as the control imposes a torque, higher order harmonic induced currents are measured on the unpowered three-phase than the previously measured signal. Down is shown a zoom of the three-phase signal measured over the period when there is no torque required.

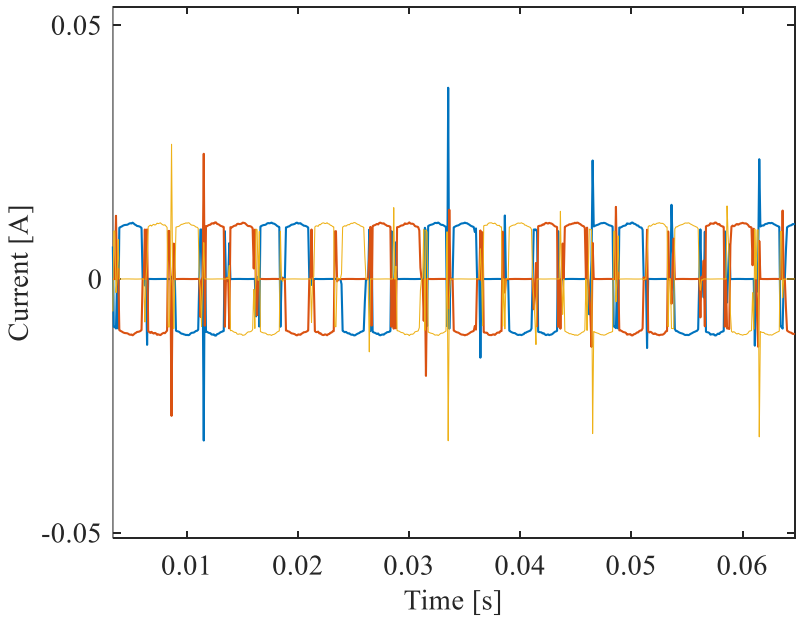

Figure 65 - Zoom on XYZ current

Apart from the computational artifices that the model introduces mathematically, the difference between the currents demonstrates the influence of the active three-phase on the inactive one, on which would be prior suitable filtering measures the induced currents. Conversely, the presence of the inactive phases also plays a role on the active one, in fact by going to look at the waveform of the ABC sign it is still possible to go and recognize the carrier sinusoid, but it is also possible to find the influence of the higher harmonics that disturb the current waveform.

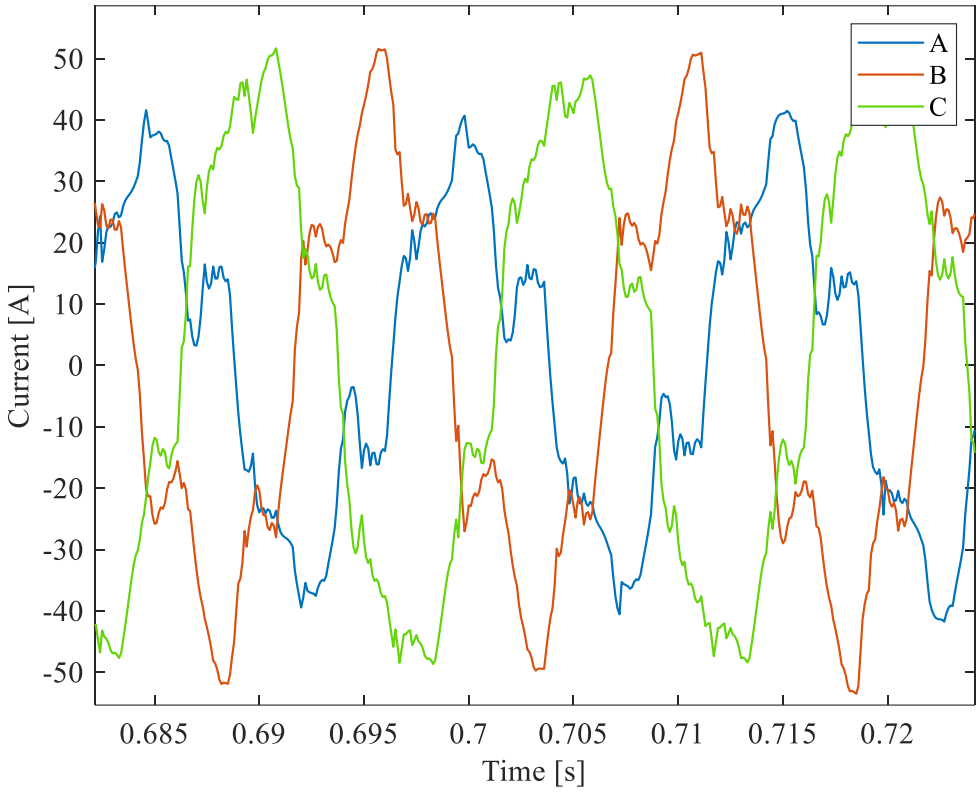

Figure 66 - ABC current

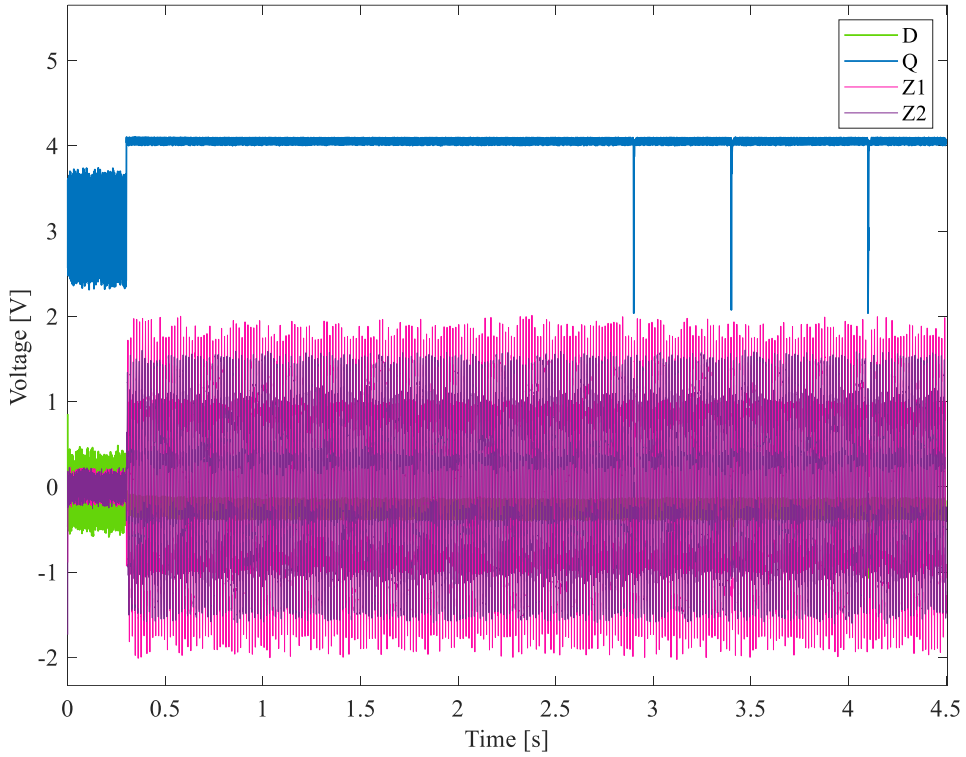

Figure 67 - Voltage dqz1z2

From the graph of the voltages in DQZ1Z2 axes, it can be seen how the control loses its effectiveness and how all the voltage delivered by the one inverter present is dispersed in the variation in Z1 and Z2, the three-phases have a completely unbalanced load.
For clarity that model summarizes the two three-phases into a single motor, creating two parallel controls, one could easily decouple the control voltages and better analyze the response, which here is naturally summed.

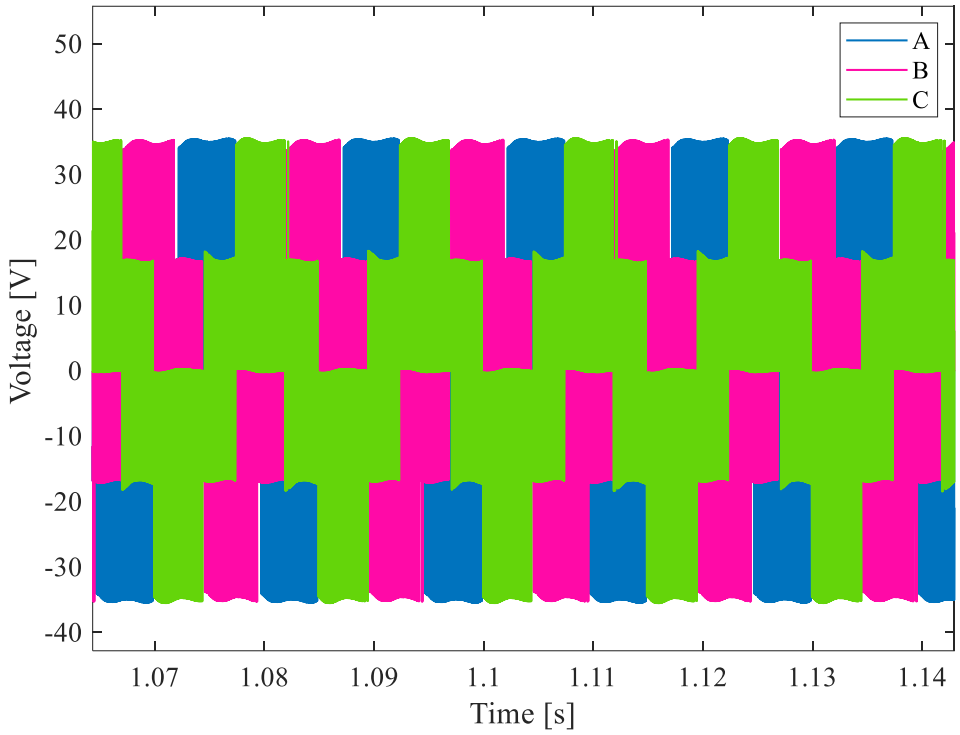

Figure 68 - ABC voltage

Above the voltage graph of the correctly powered three-phase (ABC), on the bottom the measured voltage of the three-phase off (XYZ).

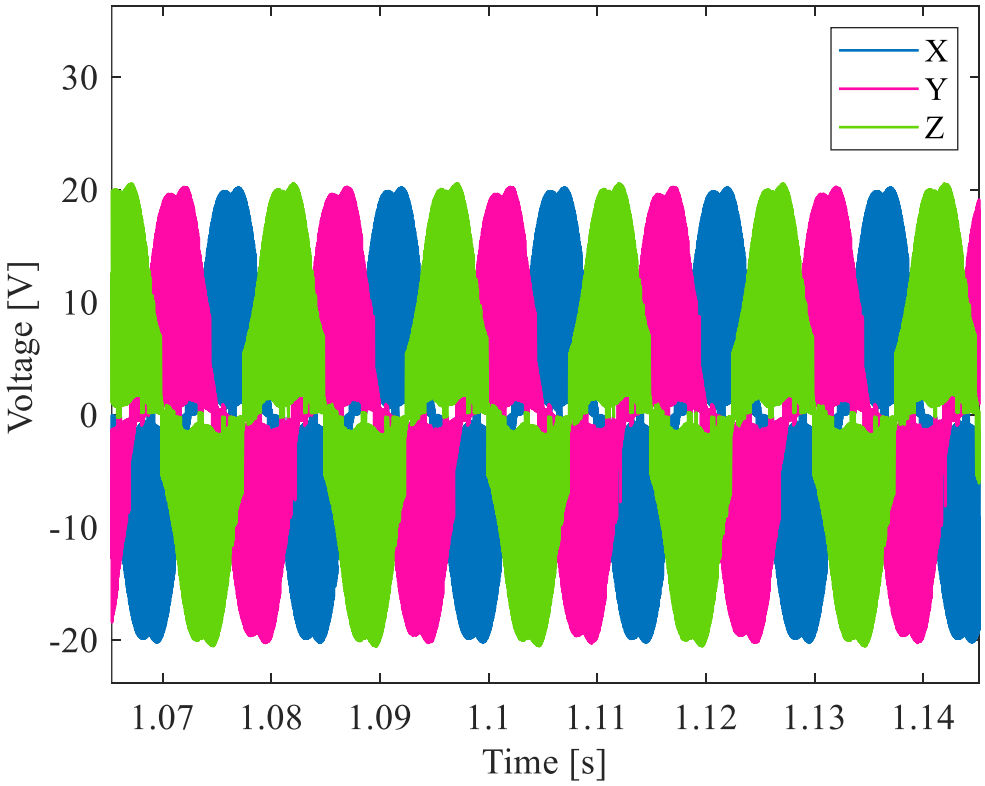

Figure 69 - XYZ voltage

5. Conclusions and future works

This thesis work explored the mathematical modelling of a six-phase low voltage motor, with the aim of building a control system in Simulink, which implemented a very accurate mathematical model of the motor. Through the implementation of the model from Ansys Motor-CAD on the Simscape block, it was possible to achieve the required goal. The main results showed how it was possible to obtain an almost complete porting of the electromagnetic model on MATLAB by comparing the simulations of the two software suites. Being able to use MATLAB and Simulink for the control and simulation of scenarios represents a great result, as the latter software has a great versatility of use. The schematic created in this way can be easily studied, updated and modified according to possible needs.

The simulation analysis has shown that the control is effective in the tested scenarios. The introduction of several measures such as the DQ limiter has allowed to improve the performance of the control scheme. The study of the current and voltage graphs, referring to the theoretical concepts present in the literature, has allowed us to identify some critical issues or possible ideas for improvements that can be easily implemented in the future thanks to the modular structure that has been developed.

5.1. Limitation

Although the values obtained from the simulations appear to be satisfactory in terms of performance, they are affected by several limitations, which did not allow a complete and exhaustive validation of the model on the model taken into consideration.

The flux data exported from Ansys Motor-CAD is based on the preliminary settings, with the rotational speed set to a single value for the electromagnetic simulation. This choice has led to limitations in the applicability of the model in Simulink for operating ranges significantly different from that used in the preliminary analyses. In particular, the model is currently not suitable for variable speed simulations. To overcome this limitation, it will be necessary to extend the analysis of electromagnetic simulations at different speeds by interpolating and subsequently integrating them into a unified model using data structure strategies. So far, the electrical machine has only been characterized at 1500 rpm, and no tests have been conducted above 3000 rpm or at non-constant speed. Therefore, no control was developed that took into account the flux weakening strategy, nor was it possible to simulate the drive-cycle for an extra-urban context that required very high operating points of the electric motor in terms of rotational speed.

Computational effort was another major limitation in the development of the project. In fact, the structure created is very demanding, so the simulations proved to be very long, and it was not possible to perform complete simulations of the drive cycles. Furthermore, for the longest simulations it was preferred to use the simplified model of the electric motor, which cannot guarantee the same adherence to reality compared to the custom Simscape block.

5.2. Future works

The project thus developed lends itself to various improvements. The main one would be the parameterization that considers the operating points used in the electromagnetic solution. To do this, it would be necessary to create a script that manages the dataset used online by comparing it with the reference. In this way it is possible to test and improve control over the entire operational range of the electric machine.

Another possible improvement would be to modify the control to a double DQ structure, to drive each three-phase separately as if there were two electric motors in one. Compared to the VDS structure, better control performance could be achieved.

For the improvement of the system's energy efficiency, as mentioned above and highlighted in the results, the implementation of a tighter control in order to limit the current in z1 and z2, which is not directly involved in the electromagnetic torque transformation process. There are studies in the literature demonstrating the effectiveness of using synchronous PI compared to classical PI to minimise current (5.1.). Consequently, the voltage load that the inverter has to devote to this component could be used to improve the maximum torque delivered by the system and speed up the transformers.

Finally, a possible future work is the implementation of an external speed measurement and control loop. In this project, an ideally generated load has always been considered. Inserting this new control variable further increases the complexity of the model, however, it is a step that must be approached to make the control realistic and applicable in a hardware plant that can carry out instrumental tests.

6. References

1.1. E. Tramacere, S. F. (2024). "Meeting Multiple Driving Needs: Design of a Novel Low Voltage Reconfigurable Electric Vehicle". *IEEE Vehicle Power and Propulsion Conference (VPPC)*, (pp. pp. 1-6). Washington, DC, USA.

1.2. Sensored Field Oriented Control of 3-Phase Permanent Magnet Synchronous Motors . ManishBhardwaj, J. 2.

1.3. Frikha, M., Croonen, J., Deepak, K., Benômar, Y., El Baghdadi, M., & Hegazy, O. (2023). Multiphase Motors and Drive Systems for Electric Vehicle Powertrains: State of the Art Analysis and Future Trends. *Energies* , (pp. 16, 768).

1.4. H. S. Che, E. L.-P. (Jan. 2014). "Current Control Methods for an Asymmetrical Six-Phase Induction Motor Drive". *IEEE Transactions on Power Electronics*, (pp. vol. 29, no. 1, pp. 407-417).

1.5. Z. Wang, Y. W. (Dec. 2018). "Decoupled Vector Space Decomposition Based Space Vector Modulation for Dual Three-Phase Three-Level Motor Drives". *IEEE Transactions on Power Electronics*, (pp. vol. 33, no. 12, pp. 10683-10697).

1.6. H. Kouki, M. B. (2014). "Vector space decomposition for double star induction machine modeling". *15th International Conference on Sciences and Techniques of Automatic Control and Computer Engineering*, (pp. pp. 581-586). Hammamet, Tunisia.

1.7. Zicheng Liu, Y. L. (JUNE 2018). A Review of Drive Techniques for Multiphase Machines. *CES TRANSACTIONS ON ELECTRICAL MACHINES AND SYSTEMS*, (pp. VOL. 2, NO. 2).

2.1. Salem, A., & Narimani, M. (2019). A Review on Multiphase Drives for Automotive. *IEEE Transactions on Transportation Electrification*.

2.2. W. N. W. A. Munim, M. J.-P. (Oct. 2017). "A unified analysis of the fault tolerance capability in six-phase induction motor drives" vol. 32, no. 10. *IEEE Trans. Power Electron. vol. 32, no. 10*, 7824-7836.

2.3. Nie, Z. (2018). *"Multiphase power electronic converters for electric vehicle machine drive systems"*.

2.4. Rubino, S., & Bojoi, R. (2024). High-Performance Torque Controllers for Multi-Three-Phase Motor Drive. *ICEM presentation*.

2.5. MATLAB, w. s. The MathWorks, Inc. (2024). MATLAB (R2024a). Natick, Massachusetts: The MathWorks, Inc.

2.6. M. Furmanik, M. S. (2022). "Analytical Exploration of Harmonics Behavior in Multiphase Machines". *International Conference on Electrical Machines (ICEM)*, (pp. pp. 2027-2033). Valencia, Spain.

2.7. Sandro, R., Radu, B., Davide, C., & Luca, Z. (2020). *Decoupled and Modular Torque Control of Multi-Three-Phase Induction Motor Drives. IEEE Transactions on Industry Applications. 56. 3831-3845. 10.1109/TIA.2020.2991122.*

2.8. Bianchi, N., & Bolognani, S. (SEPTEMBER/OCTOBER 2002). Design Techniques for Reducing the Cogging Torque in Surface-Mounted PM Motors. *IEEE TRANSACTIONS ON INDUSTRY APPLICATIONS*, (pp. VOL. 38, NO. 5).

3.1. Su, J. Y. (2012). Research on Vector Control and PWM Technique of Six-Phase PMSM. *Advanced Materials Research*, 516–517, 1626–1631.

5.1. Ruan, Z., Song, W., & Yan, A. Y. (2019). *Current Harmonic Suppression for Dual Three-Phase Permanent Magnet Synchronous Motor Drives.*

List of Figures

List of Tables